

This work is on a Creative Commons Attribution 4.0 International (CC BY 4.0) license, <https://creativecommons.org/licenses/by/4.0/>. Access to this work was provided by the University of Maryland, Baltimore County (UMBC) ScholarWorks@UMBC digital repository on the Maryland Shared Open Access (MD-SOAR) platform.

Please provide feedback Please support the ScholarWorks@UMBC repository by emailing [scholarworks-group@umbc.edu](mailto:scholarworks-group@umbc.edu) and telling us what having access to this work means to you and why it's important to you. Thank you.



# Expression profile of G-protein $\beta\gamma$ subunit gene transcripts in the mouse olfactory sensory epithelia

Aaron Sathyanesan, Adrian A. Feijoo, Saloni T. Mehta, Akua F. Nimarko and Weihong Lin\*

Department of Biological Sciences, University of Maryland Baltimore County, Baltimore, MD, USA

## Edited by:

Dieter Wicher, Max Planck Institute for Chemical Ecology, Germany

## Reviewed by:

Jean-Pierre Montmayeur, The Coca-Cola Company, USA  
Esther Alcorta, University of Oviedo, Spain

## \*Correspondence:

Weihong Lin, Department of Biological Sciences, University of Maryland Baltimore County, 1000 Hilltop Circle, Baltimore, MD 21250, USA  
e-mail: weihong@umbc.edu

Heterotrimeric G-proteins mediate a variety of cellular functions, including signal transduction in sensory neurons of the olfactory system. Whereas the  $G\alpha$  subunits in these neurons are well characterized, the gene transcript expression profile of  $G\beta\gamma$  subunits is largely missing. Here we report our comprehensive expression analysis to identify  $G\beta$  and  $G\gamma$  subunit gene transcripts in the mouse main olfactory epithelium (MOE) and the vomeronasal organ (VNO). Our reverse transcriptase PCR (RT-PCR) and realtime qPCR analyses of all known  $G\beta$  ( $\beta_{1,2,3,4,5}$ ) and  $G\gamma$  ( $\gamma_{1,2,2t,3,4,5,7,8,10,11,12,13}$ ) subunits indicate presence of multiple  $G\beta$  and  $G\gamma$  subunit gene transcripts in the MOE and the VNO at various expression levels. These results are supported by our RNA *in situ* hybridization (RISH) experiments, which reveal the expression patterns of two  $G\beta$  subunits and four  $G\gamma$  subunits in the MOE as well as one  $G\beta$  and four  $G\gamma$  subunits in the VNO. Using double-probe fluorescence RISH and line intensity scan analysis of the RISH signals of two dominant  $G\beta\gamma$  subunits, we show that  $G\gamma_{13}$  is expressed in mature olfactory sensory neurons (OSNs), while  $G\beta_1$  is present in both mature and immature OSNs. Interestingly, we also found  $G\beta_1$  to be the dominant  $G\beta$  subunit in the VNO and present throughout the sensory epithelium. In contrast, we found diverse expression of  $G\gamma$  subunit gene transcripts with  $G\gamma_2$ ,  $G\gamma_3$ , and  $G\gamma_{13}$  in the  $G\alpha_{i2}$ -expressing neuronal population, while  $G\gamma_8$  is expressed in both layers. Further, we determined the expression of these  $G\beta\gamma$  gene transcripts in three post-natal developmental stages (p0, 7, and 14) and found their cell-type specific expression remains largely unchanged, except the transient expression of  $G\gamma_2$  in a single basal layer of cells in the MOE during P7 and P14. Taken together, our comprehensive expression analyses reveal cell-type specific gene expression of multiple  $G\beta$  and  $G\gamma$  in sensory neurons of the olfactory system.

**Keywords:** olfactory sensory neurons, vomeronasal, postnatal development, sensory transduction, TRPM5, phospholipase C

## INTRODUCTION

Sensory neurons in peripheral olfactory systems employ G-protein coupled signaling pathways to transduce chemical stimuli. G-proteins are heterotrimeric, composed of three different subunits— $\alpha$ ,  $\beta$ , and  $\gamma$ . To date, gene transcripts encoding proteins of 20  $\alpha$  subunits, 5  $\beta$  subunits and 12  $\gamma$  subunits have been identified (Malbon, 2005; Dupre et al., 2009) in mammals. Out of the 20 known  $G\alpha$  subunits,  $G\alpha_{olf}$ ,  $G\alpha_s$ ,  $G\alpha_o$ , and  $G\alpha_{i2}$  subunit proteins are known to be expressed in the main olfactory system (Pace and Lancet, 1986; Jones and Reed, 1989; Wekesa and Anholt, 1999) and  $G\alpha_o$  and  $G\alpha_{i2}$  subunit proteins are known to be expressed in the vomeronasal sensory organ (VNO) (Berghard and Buck, 1996).

$G\alpha$  subunit gene expression in the MOE and VNO is regulated developmentally, and also in a cell-type specific context (Halpern et al., 1995; Sullivan et al., 1995). Post-natally, mature olfactory sensory neurons (OSNs) primarily express the stimulatory  $G\alpha_{olf}$  subunit and immature OSNs express  $G\alpha_s$  proteins (Menco et al., 1994) while  $G\alpha_o$  and  $G\alpha_{i2}$  proteins are found in the axons of OSNs (Wekesa and Anholt, 1999; Luo

et al., 2002). A differential expression pattern of  $\alpha$  subunits is also seen in vomeronasal sensory neurons (VSNs), with apical VSNs expressing  $G\alpha_{i2}$  and basal VSNs expressing  $G\alpha_o$  proteins (Halpern et al., 1995; Berghard and Buck, 1996). Mice with genetic ablation of  $G\alpha_{olf}$  and  $G\alpha_o$  from the MOE and the VNO respectively, exhibit severe deficits in olfactory-associated behaviors (Belluscio et al., 1998; Chamero et al., 2011). These studies provide strong evidence for the specific roles of each G-protein  $\alpha$  subunit, however, whether  $\beta$  and  $\gamma$  subunits can be activated in the sensory neurons of these knockout mice remains to be determined.

It has become increasingly clear in other systems, such as the cardiovascular and taste systems that following receptor activation, the  $G\beta\gamma$  dimer dissociates from the  $G\alpha$  subunit and modulates a set of downstream components that are different from those activated by  $G\alpha$  (Dingus et al., 2005; Smrcka, 2008). For example, in mammalian taste receptor cells, upon tastant binding to the taste receptor, the  $G\beta\gamma$  subunit dissociates from the  $\alpha$  subunit gustducin ( $G\alpha_{gust}$ ) and activates phospholipase C  $\beta_2$  (PLC  $\beta_2$ ) (Huang et al., 1999) which in turn activates the DAG/IP<sub>3</sub>

pathway and transient receptor potential channel M5 (TRPM5) (Oike et al., 2006; Zhang et al., 2007). Gene and protein expression data for solitary chemosensory cells (SCCs) in the gut and the respiratory tract as well as for the putative glucose-sensing hypothalamic neurons, which express taste receptor T1R1, T1R2, and T1R3, also indicates the presence of a similar G $\beta$  $\gamma$ -mediated activation of the PLC pathway (Bezencon et al., 2007; Lin et al., 2008; Ren et al., 2009; Krasteva et al., 2011). In invertebrates, G $\gamma$ <sub>1</sub> has been implicated in the detection of sugar by *Drosophila* taste neurons, and GPC-1, one of the G $\gamma$  subunit homologs in *C.elegans*, has been implicated in taste (Jansen et al., 2002) and olfactory adaptation (Yamada et al., 2009). These accumulating evidences clearly demonstrate the important role of G $\beta$  $\gamma$  subunits in chemical sensing.

In the mouse MOE, canonical mature olfactory sensory neurons (mOSNs) employ a G-protein-mediated, cAMP signal transduction cascade (Bakalyar and Reed, 1990; Munger et al., 2009). However, data regarding the expression of  $\beta$  and  $\gamma$  subunits of G-proteins in mOSNs and the epithelium, in general, is scarce and scattered. Previously, Ryba and Tirindelli (1995) reported the expression of G $\gamma$ <sub>8</sub> gene transcript in cell bodies of immature OSNs (iOSNs) using RNA in situ hybridization (RISH). In addition, G $\gamma$ <sub>13</sub> protein is known to express strongly in cilia and cell bodies of mOSNs in the MOE, including a subset of OSNs that express TRPM5, and plays an important role in olfaction (Kulaga et al., 2004; Lin et al., 2007; Li et al., 2013). More recently, Kerr et al. (2008) reported that G $\beta$ <sub>1</sub> was the dominant G $\beta$  subunit in the MOE. Boto et al. (2010) used RT-PCR to demonstrate the presence of 3 G $\beta$  and 2 G $\gamma$  subunit transcripts in the olfactory organs of *Drosophila*. Yet, to date, there is no comprehensive analysis regarding G $\beta$  $\gamma$  subunit gene expression profiles in the MOE and VNO and their developmental regulation in mammalian olfactory epithelia.

We sought to establish a cell-type specific expression profile of G $\beta$  and G $\gamma$  subunit gene transcripts in the mouse MOE and VNO. We extracted total RNA from MOE and VNO tissue and conducted *in vitro* transcription and reverse-transcriptase PCR (RT-PCR) analysis for all known G $\beta$  and G $\gamma$  subunits. We also conducted realtime quantitative PCR (qPCR) to determine quantitatively the expression levels of the G $\beta$  and G $\gamma$  subunits. In addition, we conducted RISH analysis to determine their cell-type specific expression based on the PCR results. Further, we investigated postnatal developmental changes in the gene expression pattern of various subunits in P0, P7, and P14 MOE and VNO. Our results reveal cell-type specific expression of G $\beta$  and G $\gamma$  subunit gene transcripts in the MOE and VNO, and provide a systematic analysis of the post-natal developmental profile of these subunits in peripheral olfactory epithelia.

## MATERIALS AND METHODS

### ANIMALS

Wildtype C57BL/6 mice of both sexes at different ages including post-natal day 0, 7, 14, and adult (2–4 months) were used for experiments. All animal care and procedures were approved by the Animal Care and Use Committee of University of Maryland, Baltimore County.

## REVERSE TRANSCRIPTASE PCR (RT-PCR)

### Primer design

Primers were designed to amplify a partial sequence from the 3'UTR region of each of the  $\beta$  and  $\gamma$  mRNA found in mice, such that the expected amplicons would have least homology compared to another member within the  $\beta$  and  $\gamma$  subfamilies. Primers for RT-PCR were designed using Vector NTI software (Life technologies, Carlsbad, CA) and custom-made from IDT (Coralville, IA). Primer sequences and expected sizes of amplicons are listed in **Table 1**.

### RNA extraction, cDNA synthesis and gel electrophoresis

Total RNA was extracted using Nucleospin RNA II kit (Macherey-Nagel, Dueren, Germany) from homogenized samples of freshly dissected tissue, peeled from the olfactory turbinates and vomeronasal sensory epithelium. Five hundred nanogram (ng) of total RNA template was used for cDNA synthesis using iScript cDNA Synthesis Kit (Bio-Rad, Hercules, CA) and 1  $\mu$ l of synthesized cDNA was used as starting template for PCR using specific primers against each of the five  $\beta$  and twelve  $\gamma$  subunit gene transcripts. For control of genomic DNA contamination, we omitted the reverse transcriptase (RT) in the cDNA synthesis step, which resulted in no visible PCR products (data not shown). The PCR products were run on a 2% agarose gel and viewed using a UV transilluminator. Gel images were captured using MultiDoc-It™ Imaging System (UVP, Upland, CA).

### REALTIME QUANTITATIVE PCR (QPCR)

For realtime PCR, reverse primer sequences for each of the  $\beta$  and  $\gamma$  are furnished in **Table 2**. The same forward primer used for regular reverse transcriptase PCR, was used in the qPCR reaction. Maxima SYBR Green/ROX qPCR Master Mix (Thermo Scientific, Waltham, MA) was used to perform qPCR in an iCycler IQ Real-Time Detection system (Bio-Rad). The qPCR data were analyzed using the relative quantification method ( $2^{-\Delta\Delta C_t}$ ) described by Livak and Schmittgen (2001) with *Gapdh* gene expression serving as the internal reference following the manufacturer's instruction manual.

### RNA In situ HYBRIDIZATION (RISH)

#### RNase-free conditions

All solutions used as a part of RISH, until the post-hybridization washes, were made using water treated with diethyl pyrocarbonate (DEPC; Sigma-Aldrich Co., St. Louis, MO) to a final concentration of 0.1%, stirred overnight, and autoclaved to remove excess DEPC. In general, RNase-free conditions were maintained (e.g., using RNase Zap [Sigma] for tabletops) for all RNA-related work including riboprobe synthesis.

#### Tissue preparation

The procedure for tissue preparation was modified from our previous studies (Ogura et al., 2010, 2011). Briefly, mice (P7, P14, and adult) were anesthetized using Avertin (250  $\mu$ g/g body weight), transcardially perfused with 0.1 M phosphate buffer (PB), followed by 4% paraformaldehyde (PFA) buffered in PB. P0 mice were anesthetized by hypothermia and then perfused. The nose was harvested, post-fixed for 2 h, and then further

**Table 1 | RT-PCR oligonucleotide primer sequences for Gβγ subunits.**

Gene symbol	NCBI GI no.	RT-PCR primer sequence (5' = Forward; 3' = Reverse)	Expected amplicon size (bp)
<b>Gβ SUBUNITS</b>			
<i>Gnb1</i> (β <sub>1</sub> )	111186467	5': CCTGGACATGGCAAAGAGAATACAG 3': CCTCATGTCAAAGTGGTTTATTACATC	200
<i>Gnb2</i> (β <sub>2</sub> )	141803173	5': TGCCCATGCCACACTACAGG 3': CAGAGTTGGAAGTGGTTCCTTTAT	335
<i>Gnb3</i> (β <sub>3</sub> )	20502975	5': GGAGGCTAGAGGAAGAGGTGGGAA 3': GGGGAAGGAAGCCAGGAGACTAGG	367
<i>Gnb4</i> (β <sub>4</sub> )	145301555	5': TTCTGTTCTCCAATGATACCTGG 3': ATGAATACCCTGGCCTTTGACC	236
<i>Gnb5</i> (β <sub>5</sub> )	158518005	5': CTCGTGTAGATATGACTTCTCCATGAG 3': GAAGACAGACTAGATCCAAGGAAAC	292
<b>Gγ SUBUNITS</b>			
<i>Gng1</i> (γ <sub>1</sub> )	142366390	5': GGAAGTGACACTGGAGAGAATGAT 3': CCAGCCTGGTCTACAGAGTG	545
<i>Gng2</i> (γ <sub>2</sub> )	84490416	5': GCCAGCAACAACACCGCCAG 3': ATGTCCCAGGAGCCCCAACAC	256
<i>Gngt2</i> (γ <sub>2t</sub> )	113461991	5': CCCACCCTCACCACCATCAC 3': TTTTCTCAGCATCTTTATTT	115
<i>Gng3</i> (γ <sub>3</sub> )	84579907	5': CCCCCGTTAACAGCACTATG 3': TCAGAGGAGGTCCACCGCTCT	236
<i>Gng4</i> (γ <sub>4</sub> )	31542900	5': AAGGAAGGCATGTCTAATAACAGCAC 3': ACAGCAGGAAAGGGCCCG	260
<i>Gng5</i> (γ <sub>5</sub> )	84579905	5': TTCTTCTAGCGTCGCCGCCA 3': GGTTCATGAAAAGTGGTTTGAGA	239
<i>Gng7</i> (γ <sub>7</sub> )	84579914	5': GCGCATTGAAGCTGGA 3': GAGATGGGGAAGAGAGAGAGA	189
<i>Gng8</i> (γ <sub>8</sub> )	84579910	5': TGGCCAAGATTGCTGAGG 3': GGATTCATACTTCTGCGGGGG	243
<i>Gng10</i> (γ <sub>10</sub> )	84490417	5': TTCCGGGGCCAGCGTGA 3': GCGAGCTTCTCCAGTCT	221
<i>Gng11</i> (γ <sub>11</sub> )	40254516	5': CGCAAAGAAGTCAAGTTGCAG 3': ATTTCCCTCCCCAGAGTT	177
<i>Gng12</i> (γ <sub>12</sub> )	142363813	5': TCCAGCAAGACGGCAAGC 3': CAGGTTGCTGCTGTGGTTTGCG	267
<i>Gng13</i> (γ <sub>13</sub> )	157951662	5': ATGGAGGAGTGGGATGTGC 3': TCATAGGATGGTGCACCTTG	204

fixed overnight at 4°C in 4% PFA containing 25% sucrose. After overnight fixation, the nose was deboned and embedded with optimal cutting temperature (OCT) compound (Sakura Finetek, USA Inc., Torrance CA). The embedded nose was cut into 14 μm-thick coronal sections using a cryostat (Microm international, Walldorf, Germany) and mounted onto Superfrost plus slides

(Fisher Science, Pittsburgh, PA). Slides were stored in a −80°C freezer till use.

#### **Riboprobe synthesis**

Riboprobes were synthesized using a protocol adapted and modified from Ishii et al. (2004). Briefly, RT-PCR amplicons of β

**Table 2 | qPCR reverse oligonucleotide primer sequences for Gβγ subunits.**

Gene symbol	Reverse (3') primer for qPCR
<b>Gβ subunits</b>	
<i>Gnb1</i> (β <sub>1</sub> )	AGGTGAAAAGGGTACAGGGTGCAG
<i>Gnb2</i> (β <sub>2</sub> )	GGTATGGGAGCAGGACCGGAGG
<i>Gnb3</i> (β <sub>3</sub> )	GACTGACCCTAAGGAGACGGGGC
<i>Gnb4</i> (β <sub>4</sub> )	GCAAATAGAAGGTAGAGGGTTGG
<i>Gnb5</i> (β <sub>5</sub> )	ACACTGGACGGGGTGAGTGAGTG
<b>Gγ SUBUNITS</b>	
<i>Gng1</i> (γ <sub>1</sub> )	AGAGGGTCTTCTCCAGACG
<i>Gng2</i> (γ <sub>2</sub> )	TGGTCCTTAGGTATCCAGTACA
<i>Gngt2</i> (γ <sub>2t</sub> )	TGGTCCTTAGGTATCCAGTACA
<i>Gng3</i> (γ <sub>3</sub> )	GCCTTGGACACCTTTATCCGGCA
<i>Gng4</i> (γ <sub>4</sub> )	TCACCCTGTCCATGCAGGCTTC
<i>Gng5</i> (γ <sub>5</sub> )	ACCTTCACGCGGTTGAGCCC
<i>Gng7</i> (γ <sub>7</sub> )	AGCAAGGGATCGTTGCGGGC
<i>Gng8</i> (γ <sub>8</sub> )	GCTGCTGCCTGCGACACCTT
<i>Gng10</i> (γ <sub>10</sub> )	AGCTCTGCAGCTGCCTGGGA
<i>Gng11</i> (γ <sub>11</sub> )	ATTTCCCTCCCCAGAGTT
<i>Gng12</i> (γ <sub>12</sub> )	GCTTCCAATCTCAGCTGCTGCAC
<i>Gng13</i> (γ <sub>13</sub> )	GCTCGGGGATGGTCTTGACG

and γ subunit gene transcripts detected in the MOE and the VNO were cloned into pGEMT-Easy vector (Promega, Fitchburg, WI). The plasmid was then linearized using restriction enzymes *NdeI* or *SphI* (New England Biolabs, Ipswich, MA) to make antisense and sense riboprobes depending on orientation of insert in PGEMT-Easy (i.e., if the insert had ++ orientation, then *SphI*-linearized plasmid was used to make antisense riboprobe and *NdeI*-linearized plasmid was used to make sense riboprobe, else, if the insert orientation was +/-, then the method was switched). The linearized plasmids were then used as templates in an *in vitro* transcription reaction, containing either digoxigenin-UTP (DIG) or fluorescein-UTP (FLU) to generate required antisense (+/+; *SphI*; Sp6 RNA polymerase [Thermo Scientific]) and sense riboprobes (+/+; *NdeI*; T7 RNA polymerase [Thermo Scientific]). The riboprobes were purified, dissolved in DEPC-treated water and stored at -20°C till use.

### Probe hybridization

The protocol described in Ishii et al. (2004) was modified for probe hybridization and post-hybridization washes (Ishii et al., 2004). Briefly, following an initial fixation step for 15 min in 4% PFA, slides containing tissue sections were washed in PBS and subjected to 30 min of hydrogen peroxide (0.1% in PBS) treatment to quench endogenous peroxidases. Sections were then incubated in proteinase K solution (10 μg/ml in TE) for 7 min, subsequently fixed again in 4% PFA for 10 min, acetylated for 10 min followed by sequential dehydration (90 s each) with increasing concentrations of ethanol. After equilibration in hybridization solution, riboprobes dissolved in hybridization solution were applied to each slide (0.2 μg/ml of stock probe; 200 μl/slide). A piece of parafilm was placed over slides and placed in a moist hybridization chamber, which was transferred

into a preheated 65°C incubation chamber and allowed to hybridize overnight (12–16 h).

### Probe detection

After post-hybridization washes, slides were equilibrated in 10% Normal donkey serum (in TN buffer). Anti-digoxigenin antibody (anti-digoxigenin-AP, Fab fragment from sheep, 1:1000; Roche, Indianapolis, IN) alone for single-label RISH, and in combination with anti-fluorescein antibody (anti-fluorescein-POD Fab fragment from sheep, 1:150; Roche) was applied to each slide and incubated at 4°C overnight (~12 h). Post-incubation, slides were washed and equilibrated with a magnesium-based buffer (0.1 M Tris pH 9.5, 0.1 M NaCl, 50 mM MgCl<sub>2</sub>).

For single-label colorimetric RISH, 250 μl nitro blue tetrazolium/5-bromo-4-chloro-3'-indolyl phosphate (NBT/BCIP; 1 tablet/10 ml water; Sigma-Aldrich) was applied to each slide and incubated in the dark till control antisense slides developed a purple coloration in the appropriate regions of the tissue sections. Care was taken not to overexpose the slides by monitoring slides applied with sense riboprobe. Slides were washed in PBS and then mounted with Fluoromount-G (Southern Biotech, Birmingham, AL) and covered with a coverslip.

For double-label fluorescence RISH, the anti-fluorescein probe signal was first amplified using tyramide signal amplification system (TSA Biotin System, PerkinElmer, Waltham, MA). Fluorescein antibody was then detected by applying 200 μl streptavidin-Alexa 488 (1:300, Life technologies, Grand Island, NY) per slide and incubated for 30 min in a moisture chamber. Slides were then washed and 600 ml of HNPP/Fast Red solution (Roche) at working concentration was applied to each slide and incubated in the dark for 30 min. Slides were then washed and mounted using Fluoromount and covered with a coverslip.

### IMAGE ACQUISITION

For single-label colorimetric RISH, images (2048 × 2048 pixels) were taken using 4× and 20× objective lens of an Olympus BX 41 compound microscope equipped with a Retiga 4000 R digital camera (QImaging, British Columbia, Canada). Color images were captured using bright light filtered through an accessory RGB color filter (CRI Micro\*Color 2, QImaging). Image-Pro Plus 6.2 software (Media cybernetics, Bethesda, MD) was used for image capturing. For double-label fluorescence RISH, confocal fluorescence images were taken using an Olympus BX 61 epifluorescence microscope equipped with a spinning disc confocal unit and Hamamatsu Orca-AG digital camera (Hamamatsu Photonics, Japan). Slidebook 4.0 software (3i, Denver, CO) was used for confocal image capturing and processing.

### LINE INTENSITY SCAN ANALYSIS

MOE coronal section singly labeled with antisense probes against GAP43, Gβ<sub>1</sub>, and Gγ<sub>13</sub> gene transcripts, respectively were used for the analysis and RISH signal in images was quantified using a modified version of the line intensity scan protocol described in Sathyanesan et al. (2012). Briefly, RISH images (32-bit RGB color, 2048 × 2048 pixels, pixel resolution of 0.372 μm/pixel with 20× objective lens) of tissue-sections of posterior and anterior



MOE (2 images per antisense probe per mouse) were opened in NIH ImageJ (v 1.47i) and converted to an inverted image using the “invert” tool (*Edit*→*Invert*). Two individual line scans (*Analyze*→*Plot Profile*), oriented perpendicular to the tangent to the curvature of the basal lamina were obtained from each image (see **Figure 3A** insets for representative line scan regions, 56, 58, and 58  $\mu$ m epithelial length line scans in G $\beta_1$ , GAP43, and G $\gamma_{13}$  image insets respectively). In images of anterior MOE, two line scans were performed. One was acquired from the septal region and the other from the lateral edge of the dorsal arch. In images of posterior MOE, one line scan was acquired from the septal region and the other from the endoturbinates. Scan profiles were imported into OriginPro 8.6 (Student version) statistical software suite. Epithelial lengths (X axis) as well as pixel intensity values (Y axis) in the profiles were normalized to the highest respective value in each profile. Average line scan profiles were obtained for each animal (from 2 scans/image  $\times$  2 images/animal = 4 scans per animal) using the “Average Multiple Curves” tool (*Analysis*→*Mathematics*→*Average Multiple Curves*→*Open Dialog*) over the full X range, keeping the number of points constant at 500 interpolation points per averaged trace, using linear interpolation. 500-datapoint averages were then normalized within an animal and averaged over three animals, keeping the number of points constant at 100 for the final averaged trace and reporting SEM per point. Area integrals between specified points were calculated using the “Integrate” gadget in OriginPro 8.6 (*Gadgets*→*Integrate*).

### STATISTICAL ANALYSIS

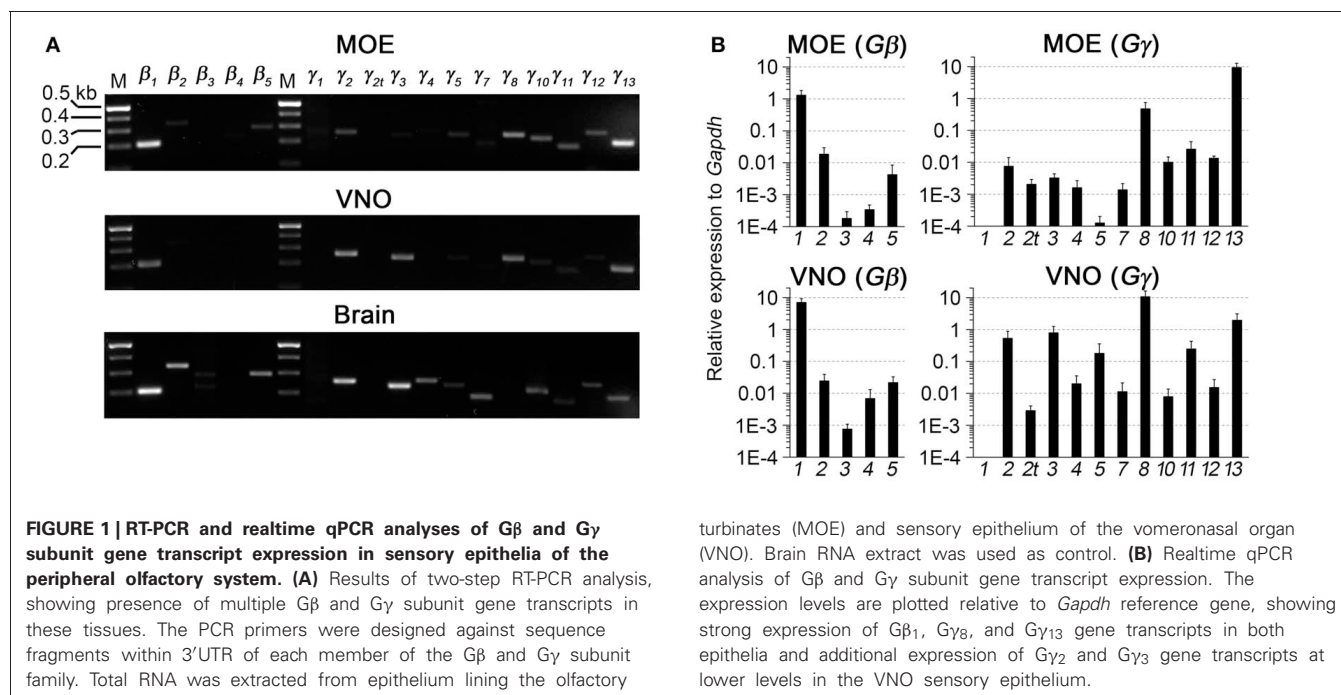
Kolmogorov-Smirnov test was used to determine the significant difference between G $\beta_1$  distribution and G $\gamma_{13}$  distribution within the GAP43 label ( $x_1 = 0.63$  to  $x_2 = 0.93$ ). For qPCR data analysis, One-way ANOVA followed by Tukey’s *post-hoc* analysis

was performed to determine statistically significant differences in the expression among G $\beta$  and G $\gamma$  subunit gene transcripts. All statistical analyses were carried out using OriginPro 8.6 software.

## RESULTS

### RT-PCR ANALYSIS OF G $\beta$ AND G $\gamma$ GENE TRANSCRIPT EXPRESSION IN SENSORY EPITHELIA OF THE PERIPHERAL OLFACTORY SYSTEM

We first performed a coarse screening for the expression of G-protein  $\beta\gamma$  subunit gene transcripts in the main and accessory peripheral olfactory systems of mouse using RT-PCR. G $\beta$  subunit members share 51–88% homology and G $\gamma$  members share 27–76% homology (Dupre et al., 2009). To maximize our chances of obtaining unique fragments for each G $\beta$  and G $\gamma$  subunit, we generated oligonucleotide primers specific to the 3’ UTRs of each of the G $\beta$  and G $\gamma$  gene transcript sequences to amplify regions that had lowest sequence homology (**Table 1**). Two-step RT-PCR was conducted using total RNA extracted from epithelium lining the mouse olfactory turbinates and vomeronasal sensory epithelium. Total RNA obtained from brain tissue was used as control. **Figure 1A** shows the RT-PCR results. In the MOE, we detected a strong band of amplicant product of G $\beta_1$ , moderate band of G $\beta_2$ , and weak bands of G $\beta_4$  and G $\beta_5$  gene transcripts. Of the 12 known G $\gamma$  subunits expressed in mammals, strong bands of amplicant products of G $\gamma_8$  and G $\gamma_{13}$  gene transcripts were observed in the MOE. We also observed moderate bands for G $\gamma_2$ , G $\gamma_{10}$ , G $\gamma_{11}$ , G $\gamma_{12}$ , and faint bands for G $\gamma_3$  and G $\gamma_5$  gene transcripts. In the VNO, RT-PCR results show a strong band of G $\beta_1$  and a weak band corresponding to G $\beta_2$  gene transcript. Among the G $\gamma$  subunits, we found strong bands for G $\gamma_2$ , G $\gamma_3$ , G $\gamma_8$ , and G $\gamma_{13}$  amplicants and very faint band for G $\gamma_5$ , G $\gamma_{10}$ , G $\gamma_{11}$ , and G $\gamma_{12}$  gene transcripts. For positive control, we used mRNA extracted from mouse brain (**Figure 1A**) and for some primers,



such as G $\gamma_1$ , we also used mRNA extracted from mouse eye tissue including the retina (**Figure A1**). The detected subunit sequence fragments were cloned into pGEM-T Easy vector and their identities were confirmed by sequencing. Thus our strategy of using primers to amplify specific 3' UTR regions allowed us to obtain sequences highly specific to each G $\beta$  and G $\gamma$  subunit. Our RT-PCR data suggests presence of multiple G $\beta$  and G $\gamma$  subunit gene transcripts in the MOE and VNO.

#### QUANTITATIVE ANALYSIS OF G $\beta$ AND G $\gamma$ GENE TRANSCRIPT EXPRESSION IN ADULT MOE AND VNO

The significant variation in the band intensity of our RT-PCR results implicates different levels of G $\beta$  and G $\gamma$  gene transcript expression. To obtain a quantitative measurement, we conducted qPCR to determine their expression relative to the glyceraldehyde 3-phosphate dehydrogenase (*Gapdh*) transcript. The specificity of the qPCR primers and products were determined by melting curve measurement, which show a single sharp peak for each subunit, indicating the primers and products are specific to our interest (**Figure A2**). In concordance with our RT-PCR results, qPCR on MOE extracts revealed a 1.3-fold higher relative expression for G $\beta_1$  and a 0.5- and 9.3-fold higher expression for G $\gamma_8$  and G $\gamma_{13}$  gene transcripts respectively. Other G $\beta$  and G $\gamma$  subunit gene transcripts were present in significantly lower quantities (One-Way ANOVA with Tukey's *post-hoc* analysis,  $p < 0.01$ ,  $n = 3$  mice) (**Figure 1B**, MOE). Similarly, in the VNO, we observed a 7-fold higher relative expression for G $\beta_1$  and significantly lower expression for all other G $\beta$  subunit gene transcripts ( $p < 0.01$ ,  $n = 3$  mice). Among G $\gamma$  subunits, we observed a 10.7-fold higher expression for G $\gamma_8$  (One-Way ANOVA with Tukey's *post-hoc* analysis,  $p < 0.01$ ,  $n = 3$  mice) and 0.5-, 0.8- and 1.9-fold higher expression for G $\gamma_2$ , G $\gamma_3$ , and G $\gamma_{13}$  gene transcripts, respectively (**Figure 1B**, VNO). These qPCR results support our initial finding from the RT-PCR experiments and further demonstrate differential expression among G $\beta$  and G $\gamma$  gene transcripts with G $\beta_1$  being the most dominant G $\beta$  in both MOE and VNO and G $\gamma_{13}$  and G $\gamma_8$  the most dominant G $\gamma$  in the MOE and VNO, respectively.

#### DETERMINATION OF CELL-TYPE SPECIFIC EXPRESSION OF G $\beta$ SUBUNIT GENE TRANSCRIPTS IN THE ADULT MOE USING RISH

G $\beta$  subunits have been shown to be involved in important cellular functions, such as chemotaxis and development (Zwaal et al., 1996; Peracino et al., 1998). In order to identify cell-type specific spatial patterns of G $\beta$  subunit gene transcript expression in the peripheral olfactory sub-systems, we conducted RISH experiments on 14  $\mu$ m-thick coronal nasal sections under high stringency conditions, with a hybridization temperature of 65°C for G $\beta$  and G $\gamma$  transcripts detected through RT-PCR. We observed specific, strong labeling for G $\beta_1$  gene transcript in the OSN layer throughout the entire MOE (**Figure 2Aa**). Our results are in agreement with an earlier study by Kerr et al. (2008) who also used RISH to identify signaling components that might partner with Ric8B, a guanine-nucleotide exchange factor (GEF) in olfactory neurons. Further, we found that G $\beta_1$  gene transcript expression was fairly uniform throughout the MOE without any zonal bias, and is clearly absent in

the respiratory epithelium (**Figure 2Aa'**). An image of the sense control is presented for comparison (**Figure 2Ab**). A relatively higher magnification image of G $\beta_1$  gene transcript expression (**Figure 2Ac**) clearly shows that G $\beta_1$  expression is restricted in OSNs and is not in supporting cell and basal stem cell layers. These results suggest an olfactory-specific role for G $\beta_1$  in the nasal cavity.

Additionally, we found weak expression of G $\beta_2$  gene transcript in the supporting cell layer (**Figures 2Ad**: antisense; **d'**: sense control). We did not observe any labels for G $\beta_4$  and G $\beta_5$  subunit gene transcripts in the MOE (**Figures 2Ae**: antisense; **e'**: sense control of G $\beta_5$ ; G $\beta_4$  data not shown), although positive signals of these two subunits were detected in RT-PCR (**Figure 1A**). We reasoned that high stringency in hybridization temperature (65°C) might affect the efficiency of RISH in detecting the weak expression of G $\beta_4$  and G $\beta_5$  gene transcripts, hence, we performed RISH with hybridization temperatures as low as 55°C. We did not find any increase in G $\beta_4$  and G $\beta_5$  labeling (data not shown). Thus, the expression of these two subunit gene transcripts, if present at all, is very weak.

#### CELL-TYPE SPECIFIC EXPRESSION OF G $\gamma$ SUBUNIT GENE TRANSCRIPTS IN THE ADULT MOE

Unlike the G $\beta$  family, where most of its members share between 75–85% sequence homology to each other, G $\gamma$  subunits are more heterogeneous, sharing a broad range of homology in their amino acid sequences from 27% to 76% (Dupre et al., 2009). Such heterogeneity suggests that the G $\gamma$  subunits confer selectivity in signaling to the G $\beta$  $\gamma$  dimer. We performed RISH on coronal nasal sections using antisense and sense probes generated against the seven G $\gamma$  subunit gene transcripts identified by our positive RT-PCR results. We found very strong expression of G $\gamma_{13}$  gene transcript in the olfactory epithelium throughout the MOE, voiding the respiratory epithelium (**Figures 2Ba,a'**, a sense control image in **b**). A relatively higher magnification image of G $\gamma_{13}$  expression is shown (**Figure 2Bc**). Clearly, G $\gamma_{13}$  gene transcript is expressed in the OSN layer only, which is consistent with previous findings showing the expression of G $\gamma_{13}$  protein in immunolabeling experiments (Lin et al., 2007; Li et al., 2013). In the supporting cell layer, we found moderate expression of G $\gamma_2$  (**Figures 2Bd** and **d'**: antisense and sense, respectively) and very weak expression of G $\gamma_{12}$  gene transcript (**Figures 2Be** and **e'**: antisense and sense, respectively). Additionally, we observed expression of G $\gamma_2$  gene transcript in the ventral respiratory epithelium (data not shown). Our RISH analysis for G $\gamma_3$  and G $\gamma_5$  gene transcripts, for which we found weak expression in our RT-PCR and qPCR, did not indicate significant expression in the MOE (**Figures 2Bf** and **f'**: antisense and sense for G $\gamma_3$ . **g** and **g'**: antisense and sense for G $\gamma_5$ ). We conducted RISH experiments with antisense probes against G $\gamma_{10}$  and G $\gamma_{11}$ . We observed very faint, ubiquitous expression for G $\gamma_{11}$  gene transcript in the OSN layer, and absence of label in the MOE for G $\gamma_{10}$  gene transcript (data not shown), thus, although these subunit gene transcripts may be present in the MOE, their quantity may be very insignificant. Finally, our RISH result shows G $\gamma_8$  gene transcript expression in the immature OSN population located in the lower portion of the OSN layer of the MOE, confirming a previous report by Ryba and



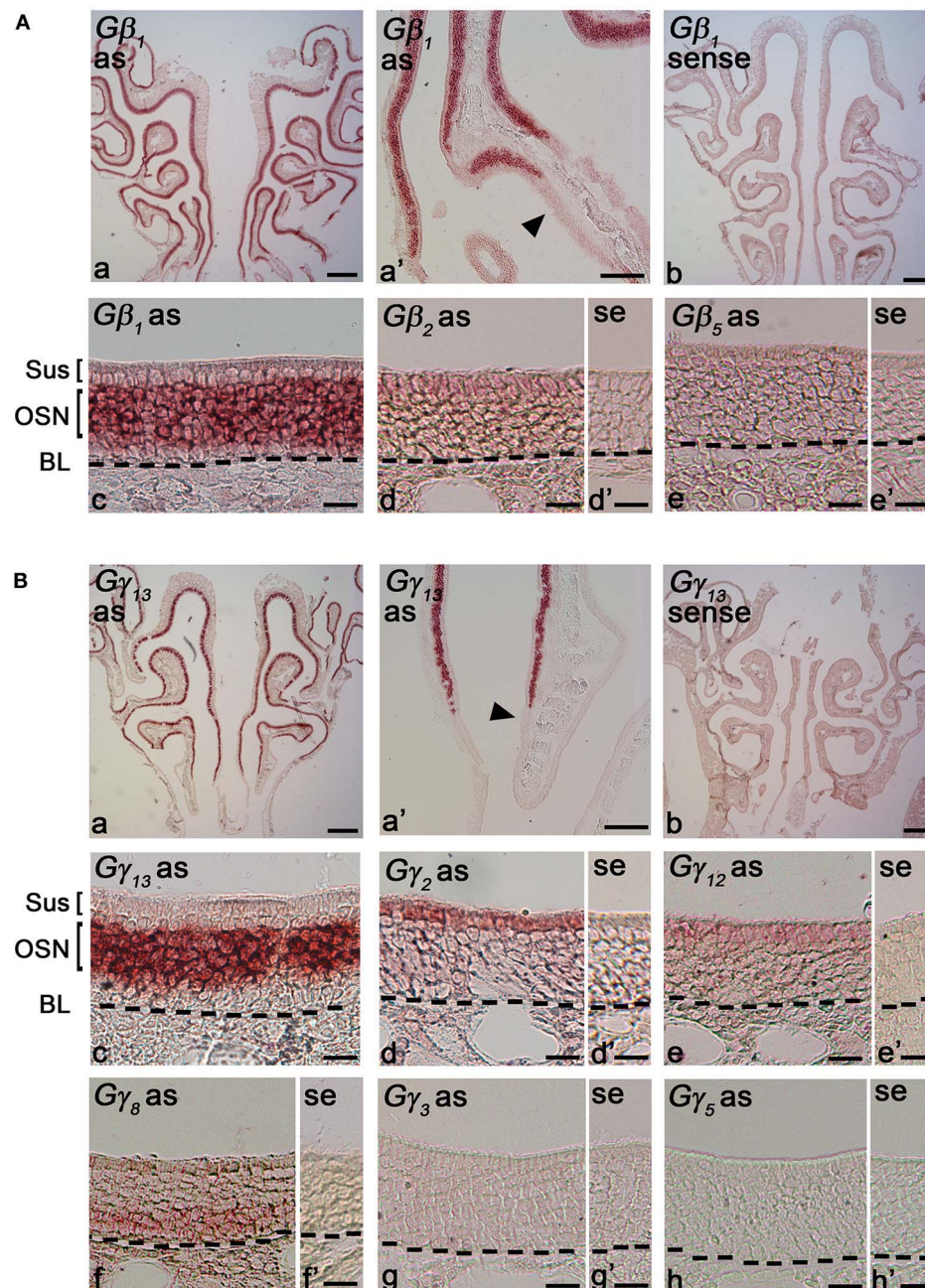


**FIGURE 2 | RNA *in situ* hybridization analysis of G $\beta$  and G $\gamma$  subunit gene transcript expression in the MOE. (A)** G $\beta$  subunit gene transcripts expression in the MOE: (a) A low magnification image of a MOE coronal section showing G $\beta_1$  gene transcript expression throughout the MOE. as: antisense probe. (a') G $\beta_1$  gene transcript expression is absent in the respiratory epithelium (arrowhead). (b) G $\beta_1$  sense probe shows no labeling. (c) Higher-magnification image of G $\beta_1$  gene transcript labeling in the MOE. Sus: sustentacular/supporting cell layer, OSN: olfactory sensory neuron layer. BL: basal lamina—black dashed line. (d and d') images of antisense and sense probe labeling of G $\beta_2$  respectively, showing weak expression in supporting cell layer. se: sense probe. (e and e') images of antisense and sense probe labeling of G $\beta_5$ , showing absence of G $\beta_5$  gene transcript. **(B)** RISH analysis of G $\gamma$  subunit gene transcripts in the MOE: (a) A low magnification image of a MOE coronal section labeled with G $\gamma_{13}$  antisense

probe, showing G $\gamma_{13}$  gene transcript expression throughout the MOE. (a') G $\gamma_{13}$  gene transcript expression is absent in the adjacent respiratory epithelium (arrowhead). (b) G $\gamma_{13}$  sense probe labeling. No signal was observed. (c) A higher-magnification image of G $\gamma_{13}$  gene transcript labeling in the MOE. (d and d') images of antisense and sense probe labeling of G $\gamma_2$ , showing G $\gamma_2$  gene transcript expression in supporting cells. (e and e') images of antisense and sense probe labeling of G $\gamma_{12}$ . The G $\gamma_{12}$  gene transcript expression in supporting cells is weak. (f and f') images of antisense and sense probe labeling of G $\gamma_8$ , showing G $\gamma_8$  gene transcript expression in immature OSN region. (g and g') images of antisense and sense probe labeling of G $\gamma_3$ . (h and h') images of antisense and sense probe labeling of G $\gamma_5$ . Note there is no labeling for both G $\gamma_3$  and G $\gamma_5$  gene transcripts in the MOE. In **(A)** and **(B)**, scale for (a, b) is 0.2 mm, (a') is 50  $\mu$ m, (c, d, d', e, e') is 20  $\mu$ m; In **(B)**, scale for (f, f', g, g', h, h') is 20  $\mu$ m.



Tirindelli (1995) (Figures 2Bf and f': antisense and sense, respectively). Thus, our RISH analysis demonstrates distinct G $\gamma$  subunit gene transcript expression in different cell types of the MOE.

Our results in Figure 2 also indicate that G $\beta$  $_1$  gene transcript expression pattern in the MOE is broader than that of G $\gamma$  $_{13}$  gene transcript. Because only G $\beta$  $_1$  gene transcript is expressed in the OSN population, we hypothesized the G $\beta$  $_1$  gene transcript is expressed in both mature and immature OSNs. We performed RISH analysis for GAP43 gene transcript, an immature OSN marker and compared quantitatively the distribution pattern of GAP43, G $\beta$  $_1$ , and G $\gamma$  $_{13}$  gene transcripts in the MOE using line scan analysis (Sathyanesan et al., 2012). We measured various regions of the MOE and examples of the measurements from

images of GAP43, G $\beta$  $_1$ , and G $\gamma$  $_{13}$  RISH are shown in Figure 3 (A: RISH images in inset; traces represent individual line scan denoted by the line segment from the apical region "a" to the basal lamina "b"—ab). We found that G $\beta$  $_1$  RISH signal distribution partially overlaps with that of GAP43 gene transcript in lower portion of the OSN layer, while in the upper 2/3 portion, it overlaps with G $\gamma$  $_{13}$  RISH signal. In contrast, we found G $\gamma$  $_{13}$  RISH signal distribution rarely overlaps with the distribution of GAP43 gene transcript signal (Figure 3C). Area integrals over the GAP43 gene transcript label (Figure 3, gray-shaded box in B and C) showed that the area covered by the G $\gamma$  $_{13}$  trace is equal to only half the area covered by the G $\beta$  $_1$  trace ( $\int G\beta_1 = 0.14$ ,  $\int G\gamma_{13} = 0.07$ ). A Kolmogorov-Smirnov test conducted between

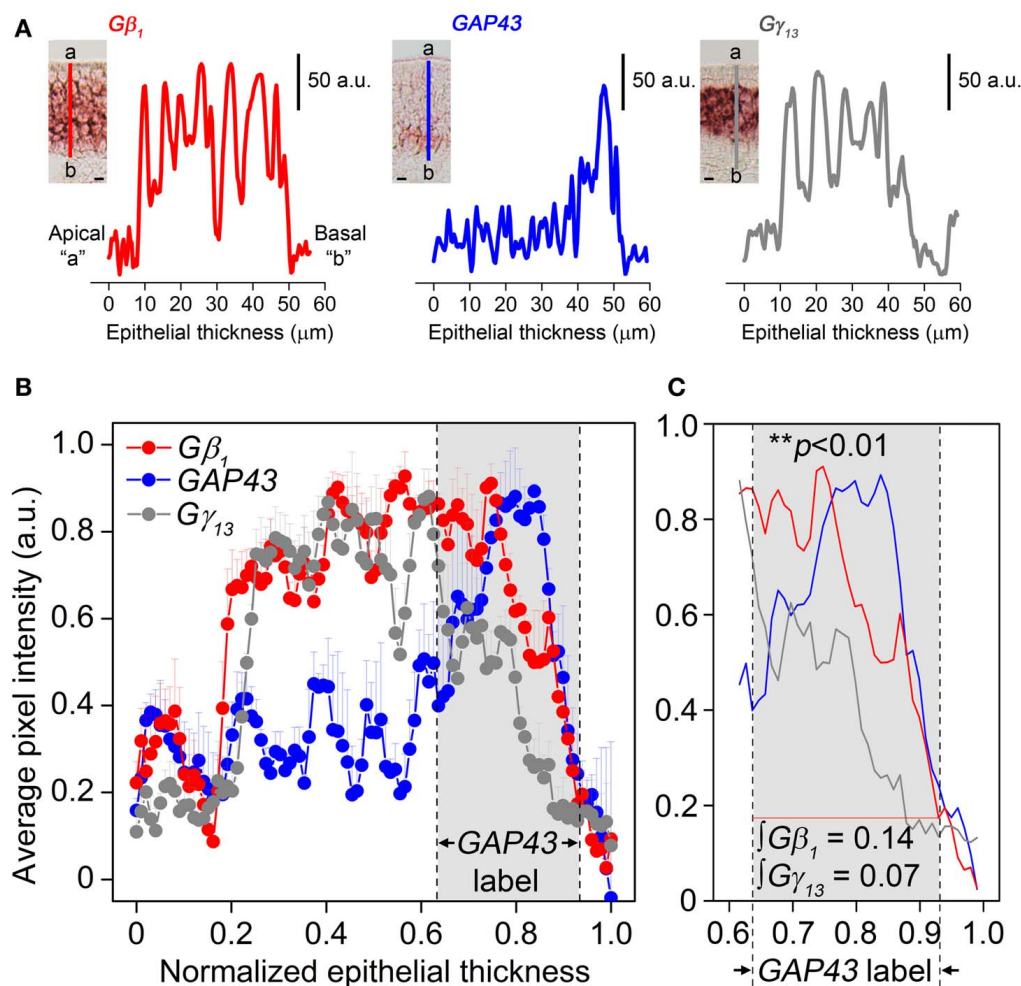


**FIGURE 3 | G $\beta$  $_1$ , GAP43, and G $\gamma$  $_{13}$  gene transcript expression distribution in the MOE analysis using line intensity scan analysis. (A)** Representative line intensity scans of RISH signals of G $\beta$  $_1$ , GAP43, and G $\gamma$  $_{13}$  antisense probe labeling corresponding to line segments marked from "a" to "b" in insets. Insets: images of typical RISH labeling. The apical region is indicated as "a" and the basal lamina indicated as "b". **(B)** Comparison of averaged line intensity scans for G $\beta$  $_1$  (red), G $\gamma$  $_{13}$  (dark grey) and GAP43 (blue) ( $n = 3$  mice per label). Error bars represent SEM on each point of averaged line scan of G $\beta$  $_1$  (red), G $\gamma$  $_{13}$  (grey) and GAP43 (blue), respectively. Light-grey shaded box between

dashed vertical lines corresponds to the region expressing GAP43. Strong, overlapping labels of G $\beta$  $_1$  and G $\gamma$  $_{13}$  are observed in the upper portion of the OSN layer, where there is no label of GAP43 gene transcript. **(C)** Magnified view of the shaded region in (B). G $\gamma$  $_{13}$  signal drops sharply and disappears, whereas G $\beta$  $_1$  signal, although is reduced, remains and significantly overlaps with GAP43 label. " $\int G\beta_1$ " and " $\int G\gamma_{13}$ " represent area integrals under G $\beta$  $_1$  (red line) and G $\gamma$  $_{13}$  (grey line). The difference between these two distributions (over which area integrals are calculated) is statistically significant (Kolmogorov-Smirnov test,  $p < 0.01$ ). Scale for insets in (A) is 10  $\mu$ m.

the G $\beta_1$  and G $\gamma_{13}$  RISH signal distributions within the GAP43 RISH label revealed a significant difference between these distributions ( $p < 0.01$ ). These results support our hypothesis that G $\beta_1$  gene transcript is expressed in both immature and mature OSNs as well as confirm that G $\gamma_{13}$  gene transcript is restricted to mature OSNs.

To further confirm our results of line scan analysis, we performed fluorescence double-label RISH. As shown in **Figure 4A**, the RISH labeling of G $\gamma_{13}$  is largely overlapped with G $\beta_1$  on the upper OSN layer, where cell bodies of mature OSNs reside, while in lower portion of the OSN layer, there are more OSNs labeled with the G $\beta_1$  probe than the G $\gamma_{13}$  probe. To confirm the line intensity scan result of the G $\gamma_{13}$  gene transcript expression pattern, we performed double labeling for G $\gamma_{13}$  and G $\alpha_{olf}$  gene transcript which is expressed in the mature OSNs and plays an essential role in odor transduction (Belluscio et al., 1998). We found their mRNA expression in largely the same population of OSNs (**Figure 4B**). These results suggest that G $\beta_1$  most likely partners with G $\gamma_{13}$  in mature OSNs and in the immature OSNs population, G $\beta_1$  partners with G $\gamma_8$ .

#### EXPRESSION OF G $\beta$ SUBUNIT GENE TRANSCRIPTS IN THE VNO

Although the transduction pathway in VSNs is considered to be mediated through phospholipase C—a known target of G $\beta\gamma$  signaling, to our knowledge, no study so far has documented the systematic expression (or lack of expression) of G $\beta$  or G $\gamma$  isoforms in the mouse VNO. We performed single-label RISH experiments to localize the expression of G $\beta$  subunit gene transcripts in VNO coronal sections. We detected strong labeling for G $\beta_1$  gene transcript in the VSN layer, including both apical and basal regions (**Figures 5a,a'**). We did not observe labeling for G $\beta_1$  gene transcript in the supporting cell layer of the vomeronasal sensory epithelium, nor did we observe labeling in the convex non-sensory epithelium. This RISH result is consistent with our RT-PCR and qPCR data, strongly suggesting that G $\beta_1$  is the dominant G $\beta$  subunit gene transcript in the VSNs.

#### EXPRESSION OF G $\gamma$ SUBUNIT GENE TRANSCRIPTS IN THE VNO

Among the subunit gene transcripts tested in our RISH analysis, we discovered expression of multiple G $\gamma$  subunit gene transcripts in VSNs including G $\gamma_2$ , G $\gamma_3$ , G $\gamma_8$ , and G $\gamma_{13}$  (**Figures 5b–e**, with **b'–e'** showing magnified images of the same subunits). Interestingly, all three subunit gene transcripts, G $\gamma_2$ , G $\gamma_3$ , and G $\gamma_{13}$  are expressed in the apical zone of the VSN layer, while G $\gamma_8$  is expressed throughout the entire VSN region. Our RISH result of G $\gamma_8$  is in agreement with an earlier study performed in rats, indicating the presence of G $\gamma_8$  in the vomeronasal sensory epithelium (Ryba and Tirindelli, 1995, 1997). However, the pattern of expression found in mice in our study was different from that seen in rats, in that we did not see increased labeling at the boundary between the sensory and non-sensory epithelia as Ryba and Tirindelli reported previously (**Figures 5d,d'**). These results from RISH analysis confirm our RT-PCR and qPCR results and further demonstrate heterogeneity in the expression of G $\gamma$  subunit gene transcripts.

VSNs in the VNO are known to express two different G $\alpha$  subunits in different zones. VSNs in the apical zone express G $\alpha_{i2}$  while VSNs in the basal zone express G $\alpha_o$ . To further characterize the zonal specific expression of the G $\beta\gamma$  subunits in the VNO, we performed fluorescence double-label RISH using G $\alpha_{i2}$  as a marker for the VSNs of the apical zone. Our results revealed that G $\beta_1$  is expressed in both G $\alpha_{i2}$ -expressing apical VSNs and G $\alpha_o$ -expressing basal VSNs (**Figures 6Aa–c**). Thus, in the mouse VNO, G $\beta_1$  most likely is the partner for both G $\alpha_{i2}$  and G $\alpha_o$  subunits. Double-label RISH analysis using probes against either G $\gamma_2$ , G $\gamma_3$  or G $\gamma_{13}$  and G $\alpha_{i2}$  revealed that these G $\gamma$  subunit gene transcripts are expressed in the apical zone of VSNs, voiding the basal zone (**Figures 6Ba–i**). Therefore, our results suggest the expression of multiple isoforms of G $\gamma$  subunit gene transcripts in the G $\alpha_{i2}$ -expressing population of VSNs and single G $\beta$  and G $\gamma$  gene transcripts (G $\beta_1$  and G $\gamma_8$ , respectively) in the basal zone of G $\alpha_o$ -expressing VSNs. **Table 3** summarizes all our results obtained from RT-PCR, qPCR and RISH.

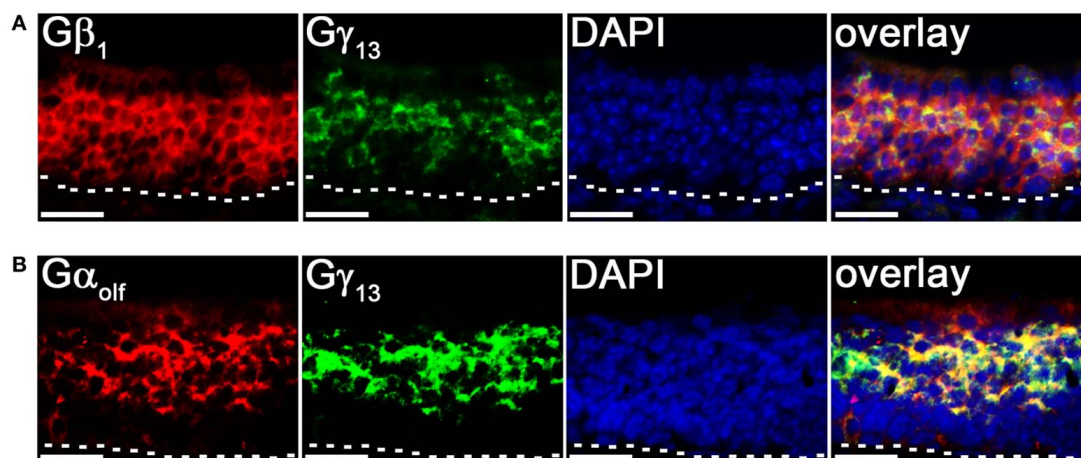


**FIGURE 4 | Cell type-specific expression of G $\beta\gamma$  subunit gene transcripts in the MOE. (A)** Confocal images of MOE labeled with G $\beta_1$  (red) and G $\gamma_{13}$  (green) fluorescent probes in double-probe RISH analysis. DAPI nuclear stain

(blue). **(B)** Confocal images of double-probe RISH analysis in MOE sections using G $\alpha_{olf}$  (red) and G $\gamma_{13}$  (green) fluorescent probes. DAPI nuclear stain (blue). White dashed lines represent basal lamina. Scale for all panels: 25  $\mu$ m.

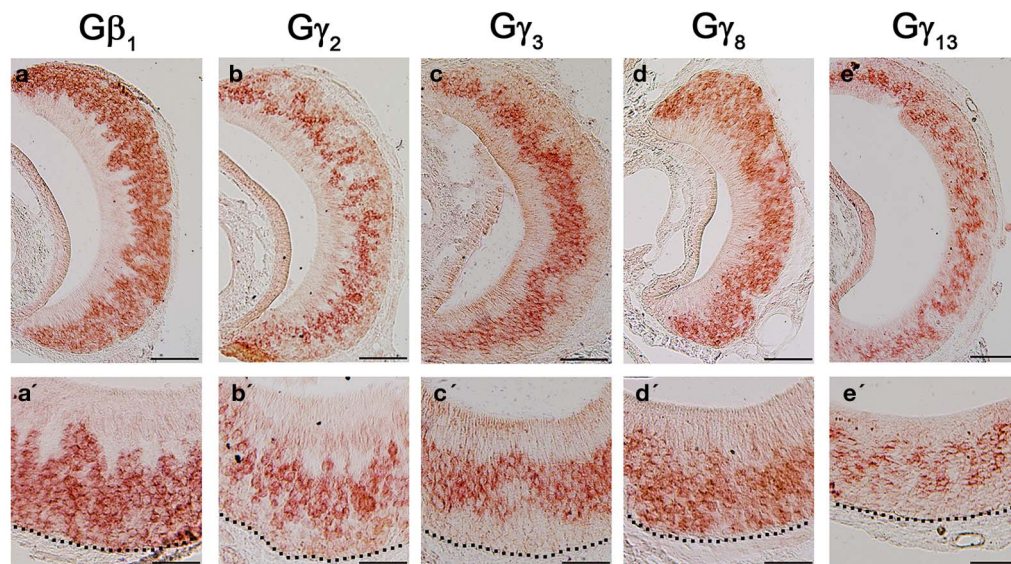


**FIGURE 5 | RNA *in situ* hybridization analysis of G $\beta$  and G $\gamma$  subunit gene transcript expression in the adult VNO. Top:** RISH images of coronal sections of VNO labeled with antisense probes against G $\beta_1$  (a), G $\gamma_2$  (b), G $\gamma_3$  (c), G $\gamma_8$  (d) and G $\gamma_{13}$  (e); **Bottom:** Higher-magnification views of RISH images

correlated to images in the top panels. Black dotted line represent basal lamina. Note that G $\beta_1$  and G $\gamma_8$  are expressed throughout VSN layers, whereas G $\gamma_2$ , G $\gamma_3$  and G $\gamma_{13}$  are expressed largely in the apical VSN zone. Scale: all top panels: 100  $\mu$ m bottom panels: 50  $\mu$ m.

#### EXPRESSION PATTERNS OF G $\beta_1$ , G $\gamma_2$ , G $\gamma_8$ , AND G $\gamma_{13}$ GENE TRANSCRIPTS IN EARLY POST-NATAL STAGES OF THE MOE

Changes in expression pattern of G-proteins in the MOE have been studied regarding G $\alpha$  subunits. It has been established that as an OSN matures, its G $\alpha$  expression profile shifts from expressing G $\alpha_s$  during immature stage to expressing G $\alpha_{olf}$  in its mature, functional stage (Imai et al., 2006; Chesler et al., 2007). Because many OSNs are mature at birth, G $\alpha_{olf}$  expression can be found abundantly in the MOE in newborn animals (Sullivan et al., 1995). Post-natal expression analysis of the G $\beta$  and G $\gamma$  subunit gene transcripts, however, has not been conducted for the mouse MOE. We extended our RISH screen of G $\beta$  and G $\gamma$  subunit gene transcripts to three post-natal developmental timepoints—P0, P7, and P14. Our results indicate an increase in the number of layers of OSNs expressing G $\beta_1$  gene transcript as the animals grow (Figures 7a–c). G $\gamma_2$  gene transcript expression was not present in P0 (Figure 7d). Unexpectedly, we observed a transient expression of G $\gamma_2$  gene transcript in a single layer of cells, which were ~1–2 cell-layers above the basal lamina at P7 and P14 (Figures 7e,f). The distribution patterns of G $\gamma_8$  and G $\gamma_{13}$  gene transcripts do not change post-natally with G $\gamma_8$  gene transcript located in the lower portion of the OSN layer (Figures 7g–i) while G $\gamma_{13}$  gene transcript is restricted in the apical region of the OSN layer (Figures 7j–l). Thus, except for the G $\gamma_2$  subunit, G $\beta_1$ , G $\gamma_8$ , and G $\gamma_{13}$  gene transcripts closely retain their distribution patterns post-natally in the MOE.

#### EXPRESSION PATTERNS OF G $\beta_1$ , G $\gamma_2$ , G $\gamma_3$ , G $\gamma_8$ , AND G $\gamma_{13}$ GENE TRANSCRIPTS IN EARLY POST-NATAL STAGES OF THE VNO

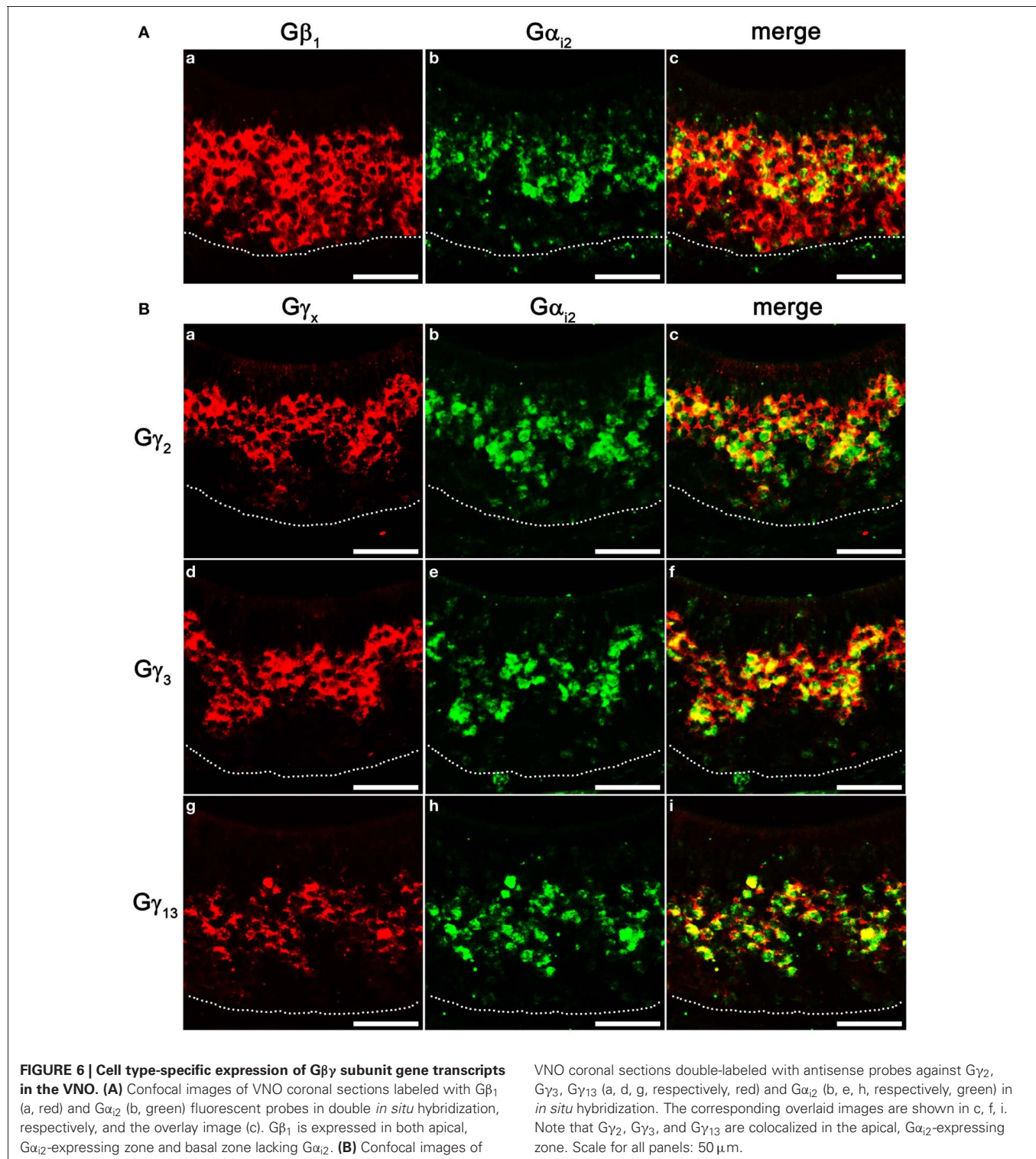
The first 2 weeks after birth involve considerable cell proliferation in the VNO and is accompanied by the topographic

targeting of the VSNs to specific regions in the accessory olfactory bulb (AOB) (Jia and Halpern, 1996; Weiler et al., 1999). Hence, we conducted our RISH analysis in P0, P7, and P14 mouse VNO sections. Our result does not show any major pattern changes in the G $\beta_1$  gene transcript expression pattern although a greater number of cells are labeled as animals become older (Figures 8a–c). There are also no major changes in the expression patterns of the apically expressed G $\gamma_2$  and G $\gamma_3$  gene transcripts, although at P0, zonal restricted distributions are not as obvious as at P14 (Figures 8d–f and g–i, respectively). In addition, we occasionally observed, for these subunits, increased labeling in the non-sensory epithelium at P0, P7, and P14 than at adult, where we did not observe significant labeling (data not shown). Similar to G $\beta_1$ , G $\gamma_8$  gene transcript, which is expressed in both apical and basal VSNs, also did not show any major changes in expression pattern (Figures 8j–l). However, we observed increased G $\gamma_{13}$  gene transcript expression as post-natal development progresses (Figures 8m–o). Thus, our results suggest that G $\beta_1$ , G $\gamma_2$ , G $\gamma_3$ , and G $\gamma_8$  gene transcripts maintain their expression patterns throughout post-natal development and G $\gamma_{13}$  gene transcript expression increases as the animal reaches adulthood.

#### DISCUSSION

We have conducted a comprehensive analysis of G $\beta\gamma$  subunit gene transcript expression profile and their postnatal developmental occurrence in the murine peripheral olfactory system using RT-PCR, qPCR and RISH approaches. Our complementary results reveal a differential expression pattern of G $\beta$  and G $\gamma$  subunits in the MOE. Whereas G $\beta_1$  is expressed in both mature and immature OSNs, G $\gamma_{13}$  is expressed exclusively in mature OSNs, contrasting the expression of G $\gamma_8$  in the immature





OSN layer. We also observed changes in the temporal expression patterns of G $\gamma_2$  which is transiently expressed between P7 and P14. In the adult VNO we observed differential labeling of G $\beta_1$ , G $\gamma_2$ , G $\gamma_3$ , G $\gamma_8$ , and G $\gamma_{13}$ . We found that G $\beta_1$  and G $\gamma_8$  are expressed in both apical and basal zones of the VSNs, whereas G $\gamma_2$ , G $\gamma_3$ , and G $\gamma_{13}$  are expressed in apical zone only. To our

knowledge, a systematic analysis of G-protein  $\beta$  and  $\gamma$  subunit gene transcript expression has not been conducted in the mouse MOE and VNO. Our analysis, therefore, enables a more complete understanding of the molecular components involved in the function and development of the mammalian peripheral olfactory system.



### EXPRESSION DIVERSITY OF Gβγ SUBUNITS

Heterotrimeric G-proteins consist of  $\alpha$ ,  $\beta$ , and  $\gamma$  subunits. In most systems, while the  $\alpha$  subunits have been studied extensively, the  $\beta\gamma$  subunits have been generally considered to play a more passive role of negatively regulating  $\alpha$  subunit activation and returning it to its ground state (Dupre et al., 2009). However, many lines of evidence have strongly established the  $\beta\gamma$  dimer as having functional roles of their own, distinct from those associated with returning the  $\alpha$  subunit to ground state. Differential expression of the 5  $\beta$  and 12  $\gamma$  subunits gene transcripts and proteins in particular mammalian cell types is an indication of specific Gβ and Gγ interactions and their unique functions. For example, in mammalian taste buds, G-protein  $\alpha$ -gustducin is expressed in taste receptor cells that can be further divided based on the types of taste receptors expressed (Hoon et al., 1999). All these cells strongly express  $\beta_3$  and  $\gamma_{13}$  transcripts, while some also express  $\beta_1$  additionally. Because in these taste receptor cells, Gβγ plays a critical role in activating the PLC  $\beta_2$ -TRPM5 signaling pathway mediating transduction of sweet, bitter, umami and fatty acid tastes (Perez et al., 2002; Zhang et al., 2007; Liu et al., 2011), addition of Gβ<sub>1</sub>, although not determined, might contribute to the coding strategy of these taste substances (Huang et al., 1999). Similarly, rod photoreceptors in the mouse visual system express  $\beta_1$ ,  $\beta_5$ -l ( $\beta_5$ -like, a splice variant of  $\beta_5$ ) and  $\gamma_1$ . The Gα-transducin- $\beta_1$ - $\gamma_1$  heterotrimer is involved in rhodopsin-mediated signal transduction (Kisselev and Gautam, 1993). Gβ<sub>5</sub>-l is found as

a partner of RGS9, which is involved in signal termination (Keresztes et al., 2004; Nishiguchi et al., 2004). Thus, expression profiling of Gβγ subunits in a particular cell type is a helpful first-step in identifying specificities and generalities in signaling mechanisms.

The expression profile of Gβγ subunit gene transcripts in the adult mouse MOE as shown by our RT-PCR and qPCR results (**Figure 1**) suggests the expression of multiple  $\beta$  and  $\gamma$  subunits, albeit at different levels. While we observed strong RT-PCR and qPCR amplification of  $\beta_1$ ,  $\gamma_8$ , and  $\gamma_{13}$ , which were reported previously (Ryba and Tirindelli, 1997; Lin et al., 2007; Kerr et al., 2008) we also noted weak or very weak levels of amplification of  $\beta_2$ ,  $\beta_4$ ,  $\beta_5$ ,  $\gamma_2$ ,  $\gamma_3$ ,  $\gamma_5$ ,  $\gamma_{10}$ ,  $\gamma_{11}$ , and  $\gamma_{12}$  gene transcripts. A study similar to ours conducted in channel catfish olfactory neurons detected a smaller number of  $\beta$  ( $\beta_1$  and  $\beta_2$ ) and  $\gamma$  subunit gene transcripts ( $\gamma_2$  and  $\gamma_3$ ) (Bruch et al., 1997). The difference between our study and the study of Bruch et al. (1997) may be due to inherent differences in the olfactory systems of the two species. In addition, differences in tissue preparation may also contribute to the observed difference. Bruch et al. (1997) used cDNA from three dissociated olfactory neurons, whereas we extracted mRNA from peeled epithelium from olfactory turbinates. For all these subunits detected in MOE tissue, we also observed positive amplification from our control brain (**Figure 1A**) or eye tissue containing the retina (**Figure A1**) except  $\beta_4$ , and  $\gamma_8$ , suggesting that our primers are efficient and specific in amplifying specific subunit gene transcripts. Because these

**Table 3 | Summary of RT-PCR, qPCR and RISH data on Gβγ expression.**

Type	RT-PCR result (quality of band)		qPCR result (normalized to <i>Gapdh</i> )		RISH analysis	
	MOE	VNO	MOE	VNO	MOE	VNO
<b>Gβ SUBUNITS</b>						
$\beta_1$	Strong	Strong	$1.31 \pm 5.13\text{E-}01$	$7.05 \pm 2.13$	mOSNs and iOSNs	Gα <sub>o</sub> -VSNs and Gα <sub>12</sub> -VSNs
$\beta_2$	Very weak	Very weak	$1.85\text{E-}02 \pm 1.11\text{E-}02$	$2.44\text{E-}02 \pm 1.50\text{E-}02$	Sus (weak)	N.D.
$\beta_3$	N.D.	N.D.	$1.81\text{E-}04 \pm 1.13\text{E-}04$	$7.58\text{E-}04 \pm 3.15\text{E-}04$	N.D.	N.D.
$\beta_4$	Very weak	N.D.	$3.39\text{E-}04 \pm 1.38\text{E-}04$	$6.82\text{E-}03 \pm 6.21\text{E-}03$	N.D.	N.D.
$\beta_5$	Weak	N.D.	$4.24\text{E-}03 \pm 4.23\text{E-}03$	$2.16\text{E-}02 \pm 1.13\text{E-}02$	N.D.	N.D.
<b>Gγ SUBUNITS</b>						
$\gamma_1$	N.D.	N.D.	$5.26\text{E-}06 \pm 3.31\text{E-}06$	$1.11\text{E-}05 \pm 7.13\text{E-}06$	N.D.	N.D.
$\gamma_2$	Weak	Strong	$7.49\text{E-}03 \pm 6.57\text{E-}03$	$5.31\text{E-}01 \pm 3.51\text{E-}01$	Sus (adult), basal cells (p7-p14)	Gα <sub>12</sub> -VSNs
$\gamma_{2t}$	N.D.	N.D.	$2.04\text{E-}03 \pm 8.53\text{E-}04$	$2.87\text{E-}03 \pm 1.18\text{E-}03$	N.D.	N.D.
$\gamma_3$	Very weak	Strong	$3.24\text{E-}03 \pm 1.10\text{E-}03$	$7.91\text{E-}01 \pm 4.48\text{E-}01$	N.D.	Gα <sub>12</sub> -VSNs
$\gamma_4$	N.D.	N.D.	$1.60\text{E-}03 \pm 1.06\text{E-}03$	$2.00\text{E-}02 \pm 1.54\text{E-}02$	N.T.	N.T.
$\gamma_5$	Weak	Very weak	$1.26\text{E-}04 \pm 7.55\text{E-}05$	$1.80\text{E-}01 \pm 1.78\text{E-}01$	N.D.	N.D.
$\gamma_7$	Very weak	N.D.	$1.37\text{E-}03 \pm 7.81\text{E-}04$	$1.13\text{E-}02 \pm 9.98\text{E-}03$	N.T.	N.T.
$\gamma_8$	Moderate	Strong	$4.75\text{E-}01 \pm 2.71\text{E-}01$	$10.7 \pm 5.53$	iOSNs	Gα <sub>o</sub> -VSNs and Gα <sub>12</sub> -VSNs
$\gamma_{10}$	Weak	Very weak	$1.01\text{E-}02 \pm 4.64\text{E-}03$	$7.90\text{E-}03 \pm 5.69\text{E-}03$	N.D.	N.D.
$\gamma_{11}$	Weak	Very weak	$2.58\text{E-}02 \pm 1.85\text{E-}02$	$2.46\text{E-}01 \pm 1.85\text{E-}01$	N.D.	N.D.
$\gamma_{12}$	Weak	Very weak	$1.34\text{E-}02 \pm 2.32\text{E-}03$	$1.53\text{E-}02 \pm 1.16\text{E-}02$	Sus (weak)	N.D.
$\gamma_{13}$	Strong	Strong	$9.34 \pm 3.38$	$1.95 \pm 1.1$	mOSNs	Gα <sub>12</sub> -VSNs

qPCR results are quantities  $\pm$  S.E.M., mOSN, mature OSN; iOSN, immature OSN; Sus, sustentacular cells; N.D., Not detected; N.T., Not tested.

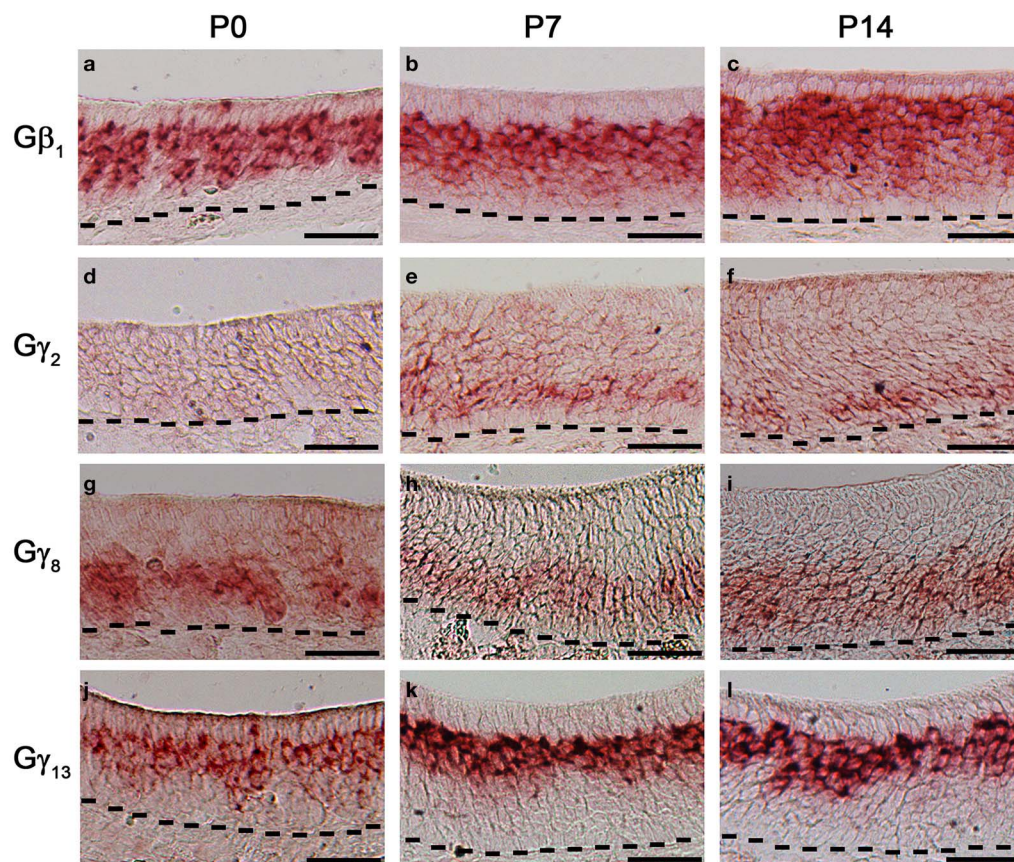


**FIGURE 7 | Post-natal expression of G $\beta_1$ , G $\gamma_2$ , G $\gamma_8$ , and G $\gamma_{13}$  gene transcripts in the MOE.** RISH images of G $\beta_1$ , G $\gamma_2$ , G $\gamma_8$ , and G $\gamma_{13}$  antisense probe labeling at post-natal stages, P0 (a, d, g, j, respectively), P7 (b, e, h, k,

respectively) and P14 (c, f, i, l, respectively). Note transient expression of G $\gamma_2$  at P7 and 14 and largely unchanged expression patterns of G $\beta_1$ , G $\gamma_8$ , and G $\gamma_{13}$ . Scale for all panels: 50  $\mu$ m.

subunits are expressed in various brain regions and because we only took a small portion of the brain in our experiments, the lack of  $\beta_4$  product in the brain control most likely is due to the weak expression of this subunit (Ruiz-Velasco et al., 2002) and the small brain tissue we used rather than the efficiency of the primers.

In our study, RT-PCR expression profiling of G $\beta\gamma$  subunits in the VNO showed the presence of a single  $\beta$  subunit gene transcript,  $\beta_1$ , and strong expression of four  $\gamma$  subunit gene transcripts,  $\gamma_2$ ,  $\gamma_3$ ,  $\gamma_8$ , and  $\gamma_{13}$ . Interestingly, Runnenburger et al. (2002) detected  $\beta_2$ ,  $\gamma_2$ ,  $\gamma_8$ , and  $\gamma_{11}$  in rat VNO using PCR and immunohistochemistry (Runnenburger et al., 2002). Again, this difference could be species related (mouse vs. rat), however, different experimental approaches may also contribute to the variation. In fact, our results from RISH analysis do not completely agree with our RT-PCR (Table 3). In our study, the RT-PCR and qPCR data reflect expression in all four cell types composing the olfactory/vomerolateral epithelium, including supporting cells, OSNs, microvillar cells and progenitor cells. While data from RISH analysis allows discriminating between the various cell-types, the two complementary approaches do not have the same sensitivity. In fact, while we observed positive labeling in most

of the subunits identified in RT-PCR screen, our RISH experiment failed to detect  $\beta_5$ ,  $\gamma_2$ , and  $\gamma_5$  gene transcripts. In addition, because we extracted mRNA from peeled epithelium, our preparation might have been contaminated with small amount of blood cells, known to express various G $\beta\gamma$  subunits (Stephens et al., 1994; Neptune and Bourne, 1997; Welch et al., 2002; Lehmann et al., 2008).

#### CELL TYPE-SPECIFIC EXPRESSION OF G $\beta\gamma$ GENE TRANSCRIPTS IN THE MOE AND VNO

Our RISH analysis of G $\beta\gamma$  gene transcript expression indicates striking similarities as well as differences between the MOE and VNO. Our data strongly demonstrate G $\beta_1$  as being the dominant G $\beta$  subunit expressed in both MOE and VNO sensory neurons which include mature and immature OSNs and VSNs, although in general the signal intensity in the mature neurons is stronger. No other G $\beta$  subunit gene transcripts were detected from MOE or VNO sensory neurons in our RISH analysis, although light expression of G $\beta_2$  gene transcript was seen in the supporting cell layer. This exclusive expression pattern is different from other sensory systems. For example, in mouse retina, G $\beta_1$  is found enriched in retinal rod cells, whereas cone cells express both G $\beta_1$



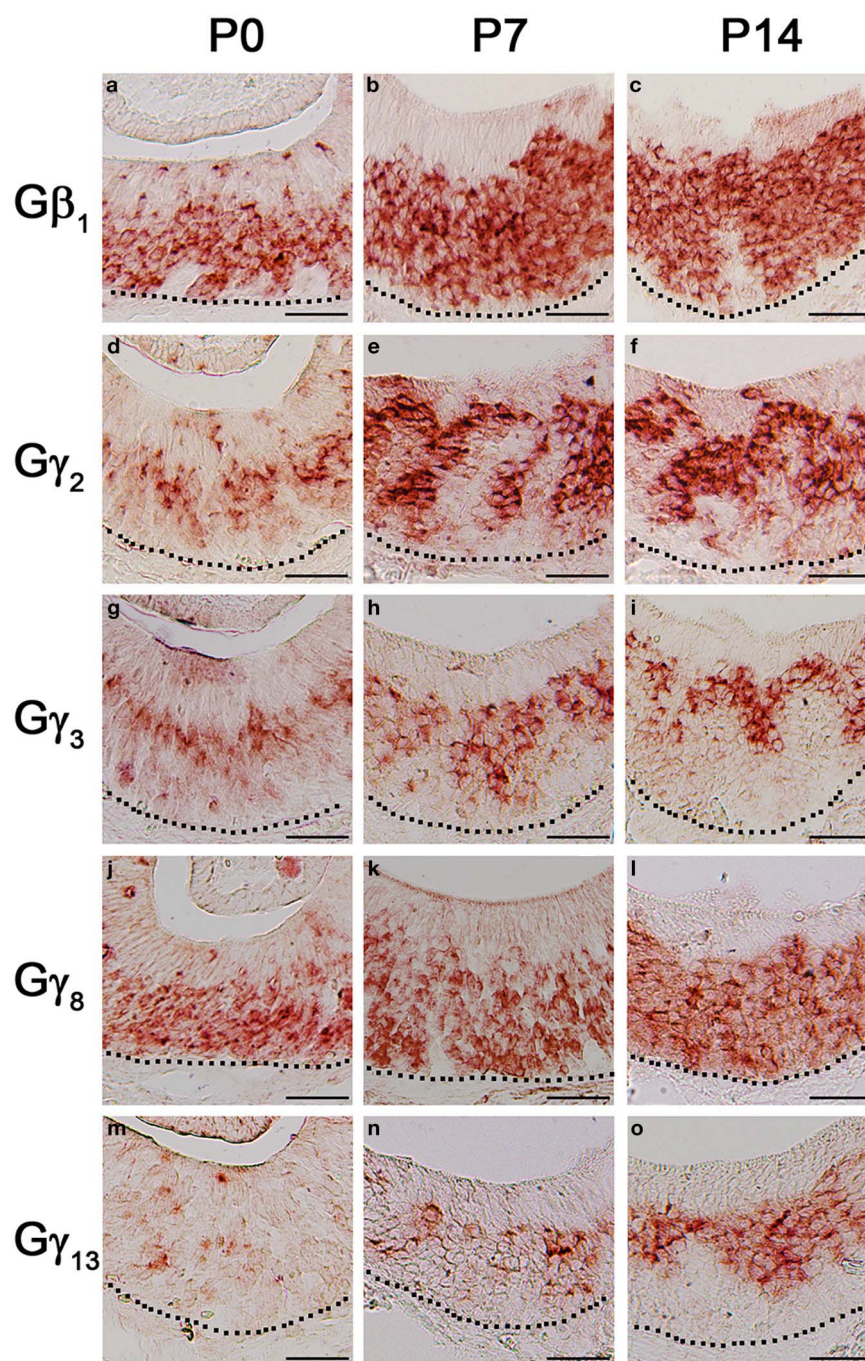


**FIGURE 8 | Post-natal expression patterns of G $\beta_1$ , G $\gamma_2$ , G $\gamma_8$ , and G $\gamma_{13}$  gene transcripts in sensory epithelium of the VNO.** RISH images of G $\beta_1$ , G $\gamma_2$ , G $\gamma_3$ , G $\gamma_8$ , and G $\gamma_{13}$  antisense probe labeling at post-natal stages, P0 (a, d, g, j, m, respectively), P7 (b, e, h, k, n, respectively) and P14 (c, f, i, l, o, respectively). The expression patterns are largely unchanged although the signals of G $\beta_1$ , G $\gamma_2$ , G $\gamma_3$ , and G $\gamma_{13}$  are increased postnatally. Scale for all panels: 50  $\mu$ m.

m, respectively), P7 (b, e, h, k, n, respectively) and P14 (c, f, i, l, o, respectively). The expression patterns are largely unchanged although the signals of G $\beta_1$ , G $\gamma_2$ , G $\gamma_3$ , and G $\gamma_{13}$  are increased postnatally. Scale for all panels: 50  $\mu$ m.

as well as G $\beta_3$  (Huang et al., 2003). Differential expression of G $\beta$  subunits is also seen among retinal bipolar cells; Rod bipolar cells express  $\beta_3$  and  $\beta_4$  and overlapping populations of cone bipolar cells express  $\beta_1$ ,  $\beta_2$ , and  $\beta_5$  (Huang et al., 2003). Such differences may be due to differences in receptor-preference for particular G-protein combinations (Kleuss et al., 1993; Wang

et al., 1997, 1999). Kerr et al. (2008) observed that G $\beta_1$  was the dominant  $\beta$  subunit in the olfactory epithelium, however, considering the relatively widespread expression of G $\beta_1$  (Malbon, 2005), it was unclear whether G $\beta_1$  was exclusive to the neuroepithelium. In serial sections from anterior to posterior MOE, we noticed that G $\beta_1$  gene transcript is exclusively expressed in

the olfactory neuroepithelium and absent from the respiratory epithelium (**Figure 2Aa'**). Boto et al. (2010) also conducted a similar search for  $\beta\gamma$  subunits in *Drosophila* olfactory receptor organs. Although the authors of this study discovered the expression of two ( $\beta_5$  and  $\beta_{13F}$ ) out of the three known *Drosophila*  $\beta$  subunits and both the  $\gamma$  subunits ( $\gamma_1$  and  $\gamma_{30A}$ ) using RT-PCR, they only investigated the spatial expression of  $\beta_{13F}$ . Our RISH results show that in the MOE, G $\beta_1$ , G $\gamma_2$ , G $\gamma_8$ , G $\gamma_{12}$ , and G $\gamma_{13}$  gene transcripts are expressed in a cell-type specific manner with G $\gamma_2$  and G $\gamma_{12}$  gene transcripts being present only in supporting cells (**Figure 2B**). Based on the exclusive and strong expression of G $\beta_1$  and G $\gamma_{13}$  and the colocalization of G $\gamma_{13}$  and G $\alpha_{olf}$  gene transcripts in mature OSNs (**Figure 3A**), we speculate that G $\beta_1$  and G $\gamma_{13}$  form a functional dimer of G $\beta_1$ - $\gamma_{13}$  and serve as the cognate partner for G $\alpha_{olf}$ . This notion is in agreement with previous findings that G $\beta_1$  and G $\gamma_{13}$  proteins are highly enriched cilia of the mature OSNs and that G $\gamma_{13}$  plays an important role in targeting other signaling proteins including G $\alpha_{olf}$  to the cilia where olfactory transduction takes place (Kulaga et al., 2004; Lin et al., 2007; Kerr et al., 2008; Liu et al., 2012; Li et al., 2013). Because G $\gamma_{13}$  and G $\alpha_{olf}$  gene transcripts are not expressed in the immature OSNs, G $\beta_1$  may form a heterotrimeric G-protein complex with G $\gamma_8$  and G $\alpha_s$ , known to be present in these cells. Since our RISH data do not provide exact cellular location of the subunit proteins, further experiments are needed to confirm whether they indeed form a dimer and partner with G $\alpha_s$  as well as to determine special functions of these dimers.

In the VNO, our results show a greater diversity in  $\gamma$  subunit gene transcript expression patterns. Surprisingly, the apical G $\alpha_{i2}$ -expressing VSNs express 4 different  $\gamma$  subunit gene transcripts— $\gamma_2$ ,  $\gamma_3$ ,  $\gamma_8$ , and  $\gamma_{13}$ , while the basal G $\alpha_o$ -expressing VSNs express only G $\gamma_8$  gene transcript. We did not observe increased labeling of G $\gamma_8$  gene transcript at the boundary between the sensory and non-sensory epithelia, as reported by Ryba and Tirindelli (1997) in rat VNO. Based on our result of strong expression of G $\beta_1$  gene transcript in both apical and basal VSNs, we speculate that different heterotrimers such as G $\alpha_{i2}$ - $\beta_1$ - $\gamma_8$ , G $\alpha_{i2}$ - $\beta_1$ - $\gamma_2$ , G $\alpha_{i2}$ - $\beta_1$ - $\gamma_3$ , G $\alpha_{i2}$ - $\beta_1$ - $\gamma_{13}$  are present in apical VSNs *in vivo*, while in basal VSNs, however, G $\alpha_o$ - $\beta_1$ - $\gamma_8$  likely is the only heterotrimer, unless hitherto undiscovered  $\beta\gamma$  subunits also exist. It is also possible that in apical VSNs, only one of the three  $\gamma$  subunit proteins may partner with G $\alpha_{i2}$ -G $\beta_1$ , even though three

gene transcripts might be expressed. Future molecular and biochemical experiments are needed to determine their interactions and identify their cognate partners in the heterotrimeric complex in these VSNs.

## DEVELOPMENTAL EXPRESSION PATTERNS OF G $\beta\gamma$ IN MOE AND VNO

Knowledge about developmental regulation of  $\beta\gamma$  subunits in mammals is limited and in the olfactory system, this knowledge is missing (Norgren et al., 1995; Chesler et al., 2007). Yet, studies from other systems in invertebrate species, such as *Drosophila* and *C.elegans* have demonstrated important roles for G $\beta$  and  $\gamma$  in development (Zwaal et al., 1996; Gotta and Ahringer, 2001; Schaefer et al., 2001; Yu et al., 2003; Izumi et al., 2004). Among mammals, Okae and Iwakura (2010) reported severe neural tube defects in mouse embryos deficient for G $\beta_1$  resulting in large-scale lethality with none of the embryos surviving more than 2 days after birth (Okae and Iwakura, 2010). Mice in which G $\beta_5$  had been genetically ablated had severe impairment in neural development of the cerebellum and the hippocampus resulting in deficiencies in motor learning and coordination (Zhang et al., 2011). These recent studies indicate that G $\beta$  and by extension,  $\gamma$  subunits, play crucial roles in mammalian neurodevelopment. In our study of postnatal expression pattern of G $\beta\gamma$  subunits, we found largely unchanged expression pattern of the majority G $\beta\gamma$  subunits tested in both the MOE and VNO, suggesting their consistent function through postnatal development to adulthood.

## CONCLUSION

In summary, we have performed comprehensive analyses of G $\beta\gamma$  subunit gene transcript expression in the mouse MOE and VNO of adults and at various stages of postnatal development. Our results reveal expression of multiple G $\beta\gamma$  subunit gene transcripts in cell-type specific fashion, which is largely unchanged from postnatal stages to adulthood, suggesting their persistent functions in sensory neurons of the peripheral olfactory system.

## ACKNOWLEDGMENTS

We thank Ms. Wangmei Luo, Julia Wolf, and Mr. Abhinav Prih for their technical assistance, and Dr. Tatsuya Ogura, Mr. David Dunston, Alex Szebenyi, Ms. Sarah Ashby for critical reading. This work was supported by NIH/NIDCD DC009269, DC012831 and ARRA administrative supplement to Weihong Lin.

## REFERENCES

- Bakalyar, H. A., and Reed, R. R. (1990). Identification of a specialized adenylyl cyclase that may mediate odorant detection. *Science* 250, 1403–1406. doi: 10.1126/science.2255909
- Belluscio, L., Gold, G. H., Nemes, A., and Axel, R. (1998). Mice deficient in G(olf) are anosmic. *Neuron* 20, 69–81. doi: 10.1016/S0896-6273(00)80435-3
- Berghard, A., and Buck, L. B. (1996). Sensory transduction in vomeronasal neurons: evidence for G alpha o, G alpha i2, and adenylyl cyclase II as major components of a pheromone signaling cascade. *J. Neurosci.* 16, 909–918.
- Bezencon, C., Le Coutre, J., and Damak, S. (2007). Taste-signaling proteins are coexpressed in solitary intestinal epithelial cells. *Chem. Senses* 32, 41–49. doi: 10.1093/chemse/bjl034
- Boto, T., Gomez-Diaz, C., and Alcorta, E. (2010). Expression analysis of the 3 G-protein subunits, Galpha, Gbeta, and Ggamma, in the olfactory receptor organs of adult *Drosophila melanogaster*. *Chem. Senses* 35, 183–193. doi: 10.1093/chemse/bjp095
- Bruch, R. C., Medler, K. F., Tran, H. N., and Hamlin, J. A. (1997). G-protein beta gamma subunit genes expressed in olfactory receptor neurons. *Chem. Senses* 22, 587–592. doi: 10.1093/chemse/22.5.587
- Chamero, P., Katsoulidou, V., Hendrix, P., Bufe, B., Roberts, R., Matsunami, H., et al. (2011). G protein G(alpha)o is essential for vomeronasal function and aggressive behavior in mice. *Proc. Natl. Acad. Sci. U.S.A.* 108, 12898–12903. doi: 10.1073/pnas.1107770108
- Chesler, A. T., Zou, D. J., Le Pichon, C. E., Peterlin, Z. A., Matthews, G. A., Pei, X., et al. (2007). A G protein/cAMP signal cascade is required for axonal convergence into olfactory glomeruli. *Proc. Natl. Acad. Sci. U.S.A.* 104, 1039–1044. doi: 10.1073/pnas.0609215104
- Dingus, J., Wells, C. A., Campbell, L., Cleator, J. H., Robinson, K., and Hildebrandt, J. D. (2005). G protein betagamma dimer formation: Gbeta and Ggamma differentially determine efficiency of *in vitro* dimer formation.



- Biochemistry* 44, 11882–11890. doi: 10.1021/bi0504254
- Dupre, D. J., Robitaille, M., Rebois, R. V., and Hebert, T. E. (2009). The role of Gbetagamma subunits in the organization, assembly, and function of GPCR signaling complexes. *Annu. Rev. Pharmacol. Toxicol.* 49, 31–56. doi: 10.1146/annurev-pharmtox-061008-103038
- Gotta, M., and Ahringer, J. (2001). Distinct roles for Gα and Gβγ in regulating spindle position and orientation in *Caenorhabditis elegans* embryos. *Nat. Cell Biol.* 3, 297–300. doi: 10.1038/35060092
- Halpern, M., Shapiro, L. S., and Jia, C. (1995). Differential localization of G proteins in the opossum vomeronasal system. *Brain Res.* 677, 157–161. doi: 10.1016/0006-8993(95)00159-N
- Hoon, M. A., Adler, E., Lindemeier, J., Battey, J. F., Ryba, N. J., and Zuker, C. S. (1999). Putative mammalian taste receptors: a class of taste-specific GPCRs with distinct topographic selectivity. *Cell* 96, 541–551. doi: 10.1016/S0092-8674(00)80658-3
- Huang, L., Max, M., Margolskee, R. F., Su, H., Masland, R. H., and Euler, T. (2003). G protein subunit Gγ13 is coexpressed with Gαo, Gβ3, and Gβ4 in retinal ON bipolar cells. *J. Comp. Neurol.* 455, 1–10. doi: 10.1002/cne.10396
- Huang, L., Shanker, Y. G., Dubauskaite, J., Zheng, J. Z., Yan, W., Rosenzweig, S., et al. (1999). Gγ13 colocalizes with gustducin in taste receptor cells and mediates IP3 responses to bitter denatonium. *Nat. Neurosci.* 2, 1055–1062. doi: 10.1038/15981
- Imai, T., Suzuki, M., and Sakano, H. (2006). Odorant receptor-derived cAMP signals direct axonal targeting. *Science* 314, 657–661. doi: 10.1126/science.1131794
- Ishii, T., Omura, M., and Mombaerts, P. (2004). Protocols for two- and three-color fluorescent RNA in situ hybridization of the main and accessory olfactory epithelia in mouse. *J. Neurocytol.* 33, 657–669. doi: 10.1007/s11068-005-3334-y
- Izumi, Y., Ohta, N., Itoh-Furuya, A., Fuse, N., and Matsuzaki, F. (2004). Differential functions of G protein and Baz-aPKC signaling pathways in *Drosophila* neuroblast asymmetric division. *J. Cell Biol.* 164, 729–738. doi: 10.1083/jcb.200309162
- Jansen, G., Weinkove, D., and Plasterk, R. H. (2002). The G-protein gamma subunit gpc-1 of the nematode *C. elegans* is involved in taste adaptation. *EMBO J.* 21, 986–994. doi: 10.1093/emboj/21.5.986
- Jia, C., and Halpern, M. (1996). Subclasses of vomeronasal receptor neurons: differential expression of G proteins (Gα2 and Gαo) and segregated projections to the accessory olfactory bulb. *Brain Res.* 719, 117–128. doi: 10.1016/0006-8993(96)00110-2
- Jones, D. T., and Reed, R. R. (1989). Golf: an olfactory neuron specific-G protein involved in odorant signal transduction. *Science* 244, 790–795. doi: 10.1126/science.2499043
- Keresztes, G., Martemyanov, K. A., Krispel, C. M., Mutai, H., Yoo, P. J., Maison, S. F., et al. (2004). Absence of the RGS9.Gβγ5 GTPase-activating complex in photoreceptors of the R9AP knockout mouse. *J. Biol. Chem.* 279, 1581–1584. doi: 10.1074/jbc.C300456200
- Kerr, D. S., Von Dannecker, L. E., Davalos, M., Michalowski, J. S., and Malnic, B. (2008). Ric-8B interacts with Gαolf and Gγ13 and co-localizes with Gαolf, Gβ1 and Gγ13 in the cilia of olfactory sensory neurons. *Mol. Cell. Neurosci.* 38, 341–348. doi: 10.1016/j.mcn.2008.03.006
- Kisselev, O., and Gautam, N. (1993). Specific interaction with rhodopsin is dependent on the gamma subunit type in a G protein. *J. Biol. Chem.* 268, 24519–24522.
- Kleuss, C., Scherubel, H., Hescheler, J., Schultz, G., and Wittig, B. (1993). Selectivity in signal transduction determined by gamma subunits of heterotrimeric G proteins. *Science* 259, 832–834. doi: 10.1126/science.8094261
- Krasteva, G., Canning, B. J., Hartmann, P., Veres, T. Z., Papadakis, T., Muhlfeld, C., et al. (2011). Cholinergic chemosensory cells in the trachea regulate breathing. *Proc. Natl. Acad. Sci. U.S.A.* 108, 9478–9483. doi: 10.1073/pnas.1019418108
- Kulaga, H. M., Leitch, C. C., Eichers, E. R., Badano, J. L., Lesemann, A., Hoskins, B. E., et al. (2004). Loss of BBS proteins causes anosmia in humans and defects in olfactory cilia structure and function in the mouse. *Nat. Genet.* 36, 994–998. doi: 10.1038/ng1418
- Lehmann, D. M., Seneviratne, A. M., and Smrcka, A. V. (2008). Small molecule disruption of G protein beta gamma subunit signaling inhibits neutrophil chemotaxis and inflammation. *Mol. Pharmacol.* 73, 410–418. doi: 10.1124/mol.107.041780
- Li, F., Ponissery-Saidu, S., Yee, K. K., Wang, H., Chen, M. L., Iguchi, N., et al. (2013). Heterotrimeric g protein subunit ggamma13 is critical to olfaction. *J. Neurosci.* 33, 7975–7984. doi: 10.1523/JNEUROSCI.5563-12.2013
- Lin, W., Margolskee, R., Donnert, G., Hell, S. W., and Restrepo, D. (2007). Olfactory neurons expressing transient receptor potential channel M5 (TRPM5) are involved in sensing semiochemicals. *Proc. Natl. Acad. Sci. U.S.A.* 104, 2471–2476. doi: 10.1073/pnas.0610201104
- Lin, W., Ogura, T., Margolskee, R. F., Finger, T. E., and Restrepo, D. (2008). TRPM5-expressing solitary chemosensory cells respond to odorous irritants. *J. Neurophysiol.* 99, 1451–1460. doi: 10.1152/jn.01195.2007
- Liu, P., Shah, B. P., Croasdel, S., and Gilbertson, T. A. (2011). Transient receptor potential channel type M5 is essential for fat taste. *J. Neurosci.* 31, 8634–8642. doi: 10.1523/JNEUROSCI.6273-10.2011
- Liu, Z., Fenech, C., Cadiou, H., Grall, S., Tili, E., Laugerette, F., Wiencis, A., et al. (2012). Identification of new binding partners of the chemosensory signaling protein Gγ13 expressed in taste and olfactory sensory cells. *Front. Cell Neurosci.* 6:26. doi: 10.3389/fncel.2012.00026
- Livak, K. J., and Schmittgen, T. D. (2001). Analysis of relative gene expression data using real-time quantitative PCR and the 2<sup>-</sup>(ΔΔC<sub>T</sub>) method. *Methods* 25, 402–408. doi: 10.1006/meth.2001.1262
- Luo, A. H., Cannon, E. H., Wekesa, K. S., Lyman, R. F., Vandenbergh, J. G., and Anholt, R. R. (2002). Impaired olfactory behavior in mice deficient in the alpha subunit of G(o). *Brain Res.* 941, 62–71. doi: 10.1016/S0006-8993(02)02566-0
- Malbon, C. C. (2005). G proteins in development. *Nat. Rev. Mol. Cell Biol.* 6, 689–701. doi: 10.1038/nrm1716
- Menco, B. P., Tekula, F. D., Farbman, A. I., and Danho, W. (1994). Developmental expression of G-proteins and adenylyl cyclase in peripheral olfactory systems. Light microscopic and freeze-substitution electron microscopic immunocytochemistry. *J. Neurocytol.* 23, 708–727.
- Munger, S. D., Leinders-Zufall, T., and Zufall, F. (2009). Subsystem organization of the mammalian sense of smell. *Annu. Rev. Physiol.* 71, 115–140. doi: 10.1146/annurev-physiol.70.113006.100608
- Neptune, E. R., and Bourne, H. R. (1997). Receptors induce chemotaxis by releasing the betagamma subunit of Gi, not by activating Gq or Gs. *Proc. Natl. Acad. Sci. U.S.A.* 94, 14489–14494.
- Nishiguchi, K. M., Sandberg, M. A., Kooijman, A. C., Martemyanov, K. A., Pott, J. W., Hagstrom, S. A., et al. (2004). Defects in RGS9 or its anchor protein R9AP in patients with slow photoreceptor deactivation. *Nature* 427, 75–78. doi: 10.1038/nature02170
- Norgren, R. B. Jr., Gao, C., Ji, Y., and Fritzsche, B. (1995). Tangential migration of luteinizing hormone-releasing hormone (LHRH) neurons in the medial telencephalon in association with transient axons extending from the olfactory nerve. *Neurosci. Lett.* 202, 9–12.
- Ogura, T., Krosnowski, K., Zhang, L., Bekkerman, M., and Lin, W. (2010). Chemoreception regulates chemical access to mouse vomeronasal organ: role of solitary chemosensory cells. *PLoS ONE* 5:e11924. doi: 10.3410/f4724956.4613054
- Ogura, T., Szebenyi, S. A., Krosnowski, K., Sathyanesan, A., Jackson, J., and Lin, W. (2011). Cholinergic microvillous cells in the mouse main olfactory epithelium and effect of acetylcholine on olfactory sensory neurons and supporting cells. *J. Neurophysiol.* 106, 1274–1287. doi: 10.1152/jn.00186.2011
- Oike, H., Wakamori, M., Mori, Y., Nakanishi, H., Taguchi, R., Misaka, T., et al. (2006). Arachidonic acid can function as a signaling modulator by activating the TRPM5 cation channel in taste receptor cells. *Biochim. Biophys. Acta* 1761, 1078–1084. doi: 10.1016/j.bbalip.2006.07.005
- Okae, H., and Iwakura, Y. (2010). Neural tube defects and impaired neural progenitor cell proliferation in Gβγ1-deficient mice. *Dev. Dyn.* 239, 1089–1101. doi: 10.1002/dvdy.22256
- Pace, U., and Lancet, D. (1986). Olfactory GTP-binding protein: signal-transducing polypeptide of vertebrate chemosensory neurons. *Proc. Natl. Acad. Sci. U.S.A.* 83, 4947–4951.
- Peracino, B., Borleis, J., Jin, T., Westphal, M., Schwartz, J. M., Wu, L., et al. (1998). G protein beta subunit-null mutants are impaired in phagocytosis and chemotaxis due

- to inappropriate regulation of the actin cytoskeleton. *J. Cell Biol.* 141, 1529–1537. doi: 10.1083/jcb.141.7.1529
- Perez, C. A., Huang, L., Rong, M., Kozak, J. A., Preuss, A. K., Zhang, H., et al. (2002). A transient receptor potential channel expressed in taste receptor cells. *Nat. Neurosci.* 5, 1169–1176. doi: 10.1038/nn952
- Ren, X., Zhou, L., Terwilliger, R., Newton, S. S., and de Araujo, I. E. (2009). Sweet taste signaling functions as a hypothalamic glucose sensor. *Front. Integr. Neurosci.* 3:12. doi: 10.3389/neuro.07.012.2009
- Ruiz-Velasco, V., Ikeda, S. R., and Puhl, H. L. (2002). Cloning, tissue distribution, and functional expression of the human G protein beta 4-subunit. *Physiol. Genomics* 8, 41–50. doi: 10.1152/physiolgenomics.00085.2001
- Runnenburger, K., Breer, H., and Boekhoff, I. (2002). Selective G protein beta gamma-subunit compositions mediate phospholipase C activation in the vomeronasal organ. *Eur. J. Cell Biol.* 81, 539–547.
- Ryba, N. J., and Tirindelli, R. (1995). A novel GTP-binding protein gamma-subunit, G gamma 8, is expressed during neurogenesis in the olfactory and vomeronasal neuroepithelia. *J. Biol. Chem.* 270, 6757–6767.
- Ryba, N. J., and Tirindelli, R. (1997). A new multigene family of putative pheromone receptors. *Neuron* 19, 371–379. doi: 10.1016/S0896-6273(00)80946-0
- Sathyanesan, A., Ogura, T., and Lin, W. (2012). Automated measurement of nerve fiber density using line intensity scan analysis. *J. Neurosci. Methods* 206, 165–175. doi: 10.1016/j.jneumeth.2012.02.019
- Schaefer, M., Petronczki, M., Dorner, D., Forte, M., and Knoblich, J. A. (2001). Heterotrimeric G proteins direct two modes of asymmetric cell division in the *Drosophila* nervous system. *Cell* 107, 183–194. doi: 10.1016/S0092-8674(01)00521-9
- Smrcka, A. V. (2008). G protein betagamma subunits: central mediators of G protein-coupled receptor signaling. *Cell Mol. Life Sci.* 65, 2191–2214. doi: 10.1007/s00018-008-8006-5
- Stephens, L., Smrcka, A., Cooke, F. T., Jackson, T. R., Sternweis, P. C., and Hawkins, P. T. (1994). A novel phosphoinositide 3 kinase activity in myeloid-derived cells is activated by G protein beta gamma subunits. *Cell* 77, 83–93. doi: 10.1016/0092-8674(94)90237-2
- Sullivan, S. L., Bohm, S., Ressler, K. J., Horowitz, L. F., and Buck, L. B. (1995). Target-independent pattern specification in the olfactory epithelium. *Neuron* 15, 779–789. doi: 10.1016/0896-6273(95)90170-1
- Wang, Q., Mullah, B., Hansen, C., Asundi, J., and Robishaw, J. D. (1997). Ribozyme-mediated suppression of the G protein gamma7 subunit suggests a role in hormone regulation of adenylyl cyclase activity. *J. Biol. Chem.* 272, 26040–26048. doi: 10.1074/jbc.272.41.26040
- Wang, Q., Mullah, B. K., and Robishaw, J. D. (1999). Ribozyme approach identifies a functional association between the G protein beta1gamma7 subunits in the beta-adrenergic receptor signaling pathway. *J. Biol. Chem.* 274, 17365–17371. doi: 10.1074/jbc.274.24.17365
- Weiler, E., McCulloch, M. A., and Farbman, A. I. (1999). Proliferation in the vomeronasal organ of the rat during postnatal development. *Eur. J. Neurosci.* 11, 700–711. doi: 10.1046/j.1460-9568.1999.00476.x
- Wekesa, K. S., and Anholt, R. R. (1999). Differential expression of G proteins in the mouse olfactory system. *Brain Res.* 837, 117–126. doi: 10.1016/S0006-8993(99)01630-3
- Welch, H. C., Coadwell, W. J., Ellison, C. D., Ferguson, G. J., Andrews, S. R., Erdjument-Bromage, H., et al. (2002). P-Rex1, a PtdIns(3, 4, 5)P3- and Gbetagamma-regulated guanine-nucleotide exchange factor for Rac. *Cell* 108, 809–821. doi: 10.1016/S0092-8674(02)00663-3
- Yamada, K., Hirotsu, T., Matsuki, M., Kunitomo, H., and Iino, Y. (2009). GPC-1, a G protein gamma-subunit, regulates olfactory adaptation in *Caenorhabditis elegans*. *Genetics* 181, 1347–1357. doi: 10.1534/genetics.108.099002
- Yu, F., Cai, Y., Kaushik, R., Yang, X., and Chia, W. (2003). Distinct roles of Galphai and Gbeta13F subunits of the heterotrimeric G protein complex in the mediation of *Drosophila* neuroblast asymmetric divisions. *J. Cell Biol.* 162, 623–633. doi: 10.1083/jcb.200303174
- Zhang, J. H., Pandey, M., Seigneur, E. M., Panicker, L. M., Koo, L., Schwartz, O. M., et al. (2011). Knockout of G protein beta5 impairs brain development and causes multiple neurologic abnormalities in mice. *J. Neurochem.* 119, 544–554. doi: 10.1111/j.1471-4159.2011.07457.x
- Zhang, Z., Zhao, Z., Margolskee, R., and Liman, E. (2007). The transduction channel TRPM5 is gated by intracellular calcium in taste cells. *J. Neurosci.* 27, 5777–5786. doi: 10.1523/JNEUROSCI.4973-06.2007
- Zwaal, R. R., Ahringer, J., Van Luenen, H. G., Rushforth, A., Anderson, P., and Plasterk, R. H. (1996). G proteins are required for spatial orientation of early cell cleavages in *C. elegans* embryos. *Cell* 86, 619–629. doi: 10.1016/S0092-8674(00)80135-X

**Conflict of Interest Statement:** The authors declare that the research was conducted in the absence of any commercial or financial relationships that could be construed as a potential conflict of interest.

Received: 10 April 2013; paper pending published: 06 May 2013; accepted: 16 May 2013; published online: 04 June 2013.

Citation: Sathyanesan A, Feijoo AA, Mehta ST, Nimarko AF and Lin W (2013) Expression profile of G-protein  $\beta\gamma$  subunit gene transcripts in the mouse olfactory sensory epithelia. *Front. Cell. Neurosci.* 7:84. doi: 10.3389/fncel.2013.00084

Copyright © 2013 Sathyanesan, Feijoo, Mehta, Nimarko and Lin. This is an open-access article distributed under the terms of the Creative Commons Attribution License, which permits use, distribution and reproduction in other forums, provided the original authors and source are credited and subject to any copyright notices concerning any third-party graphics etc.

## APPENDIX

